Computational Predicting CB2 Allosteric Binding Sites to Promote the Allosteric Modulators Design

by

Jiayi Yuan

Bachelor's Degree of Science, Shenyang Pharmaceutical University, 2020

Submitted to the Graduate Faculty of the

School of Pharmacy in partial fulfillment

of the requirements for the degree of

Master of Science

University of Pittsburgh

2022

UNIVERSITY OF PITTSBURGH

SCHOOL OF PHARMACY

This thesis or dissertation was presented

by

Jiayi Yuan

It was defended on

March 24, 2022

and approved by

Xiang-Qun (Sean) Xie, Ph.D., EMBA, Professor, Department of Pharmaceutical Sciences

Levent Kirisci, Ph.D., Professor, Department of Pharmaceutical Sciences

Junmei Wang, Ph.D., Assistant Professor, Department of Pharmaceutical Sciences

Zhiwei Feng, Ph.D., Assistant Professor, Department of Pharmaceutical Sciences

Thesis Advisor/Dissertation Director:
Zhiwei Feng, Ph.D., Assistant Professor, Department of Pharmaceutical Sciences

Copyright © by Jiayi Yuan

2022

In Silico Prediction and Validation of CB2 Allosteric Binding Sites to Aid the Design of Allosteric Modulators

Jiayi Yuan, B.S

University of Pittsburgh, 2022

Abstract: Although the 3D structures of active and inactive cannabinoid receptors type 2 (CB2) are available, neither the X-ray crystal nor the cryo-EM structure of the CB2-orthosteric ligand-allosteric modulator has been resolved, prohibiting the drug discovery and development of CB2 allosteric modulators (AMs). In the present work, we mainly focused on investigating the potential allosteric binding site(s) of CB2. We applied different algorithms or tools to predict the potential allosteric binding sites of CB2 with the existing agonists. Seven potential allosteric sites can be observed for either CB2-CP55940 or CB2-WIN 55,212-2 complex, among which sites B, C, G, and K are supported by the reported 3D structures of Class A GPCRs coupled with AMs. Applying our novel algorithm toolset-MCCS, we docked three known AMs of CB2 including Ec2la (C-2), trans-β-caryophyllene (TBC), and cannabidiol (CBD) to each site for further comparisons and quantified the potential binding residues in each allosteric binding site. Sequentially, we selected the most promising binding pose of C-2 in five allosteric sites to conduct the molecular dynamics (MD) simulations. Based on the results of docking studies and MD simulations, we suggest that site H is the most promising allosteric binding site. We plan to conduct bio-assay validations in the future.

Keywords: cannabinoid receptor 2; allosteric binding site; positive allosteric modulators; negative allosteric modulators

Table of Contents

Preface ..... **xi**

1.0 Instruction 1

1.1 The Human Endocannabinoid System (ECS) **1**

1.2 Cannabinoid Receptor 1 and Cannabinoid Receptor 2 ..... **2**

1.2.1 Distribution and Therapeutic Effects **2**

1.2.2 Structural Information **2**

1.3 Orthosteric Ligands and Allosteric Modulators **4**

1.3.1 Classification **4**

1.3.2 Development **4**

1.4 Downstream signaling pathways **5**

1.5 Endocannabinoids (eCBs) **6**

1.6 Advantages and Disadvantages of AMs **7**

1.7 Aims and work **7**

2.0 Materials and Methods **10**

2.1 3D structures of CB2 ..... **10**

2.2 Predictions of Allosteric Binding Sites of CB2 ..... **10**

2.3 Molecular Complex Characterizing System (MCCS) **11**

2.4 Molecular Dynamics (MD) Simulation **14**

2.5 Post-MD analysis **15**

3.0 Results **17**

3.1 Overview of Seven Predicted Allosteric Binding Sites of CB2 ..... **17**

3.2 Detailed Binding Poses and Interactions of AMs in Site B, K, and C of CB2..... 19

3.3 Detailed Binding Poses and Interactions of AMs in Site G of CB2..... 24

3.4 Detailed Binding Poses and Interactions of AMs in Site H of CB2..... 25

3.5 Detailed Binding Poses and Interactions of AMs in Site I and J of CB2..... 28

3.6 MD Simulations for C-2 in Five Predicted Allosteric Binding Sites..... 30

4.0 Conclusions..... 38

Bibliography..... 40

List of Tables

Table 1. The comparisons of docking scores of AMs in various allosteric binding sites(kcal/mol). 20

Table 2. Energy decomposition of MM-PBSA-WSAS free energy for the CB2/CP55940/C-2 complex. All energies are in kcal/mol. 34

Table 3. Energy decomposition of MM-PBSA-WSAS free energy for C-2 binding to CB2 with CP55940 residing in the orthosteric site. All energies are in kcal/mol. 35

Table 4. Energy decomposition of MM-PBSA-WSAS free energy for CP55940 binding to CB2 with C-2, an allosteric agonist existing. All energies are in kcal/mol. 35

List of Figures

Figure 1 CB2R AM: C-2, TBC, and CBD 15

Figure 2. Predicted allosteric binding sites of CB2 by CavityPlus, Protein Allosteric and Regulatory Sites (PARS), and Sybyl-X. The orthosteric binding site was highlighted in yellow surface, while predicted allosteric sites are highlighted in dots. 18

Figure 3 The detailed interactions and residue energy contribution of C-2, TBC and CBD in sites B, C and K. (a) The detailed binding pose of C-2 in site B. (b) The detailed binding pose of TBC in site C. (c) The detailed binding pose of CBD in site C. (d) The detailed binding pose of C-2 in site K. (e) The detailed binding pose of TBC in site K. (f) The detailed binding pose of CBD in site K. (g) The residue energy contribution of key residues for C-2 in site B. (h) The comparisons of residue energy contribution of key residues for TBC and CBD in site C. (i) The comparisons of residue energy contribution of key residues for C-2, TBC, and CBD in site K. 23

Figure 4. The detailed interactions and residue energy contribution of C-2, TBC and CBD in site G. (a) The detailed binding pose of C-2 in site G. (b) The detailed binding pose of TBC in site G. (c) The detailed binding pose of CBD in site G. (d) The comparisons of residue energy contribution of the key residues for these AMs in site G. 25

Figure 5. The detailed interactions and residue energy contribution of C-2, TBC and CBD in site H. (a) The detailed binding pose of C-2 in site H. (b) The detailed binding pose of TBC in site H. (c) The detailed binding pose of CBD in site H. (d) The comparisons of residue energy contribution of these AMs in site H. 27

Figure 6. The detailed interactions and residue energy contribution of C-2, TBC and CBD in site I. (a) The detailed binding pose of C-2 in site I. (b) The detailed binding pose of TBC in site I. (c) The detailed binding pose of CBD in site I. (d) The comparisons of residue energy contribution of binding residues for these AMs in site I. 29

Figure 7. The detailed interactions and residue energy contribution of C-2, TBC and CBD in site J. (a) The detailed binding pose of C-2 in site J. (b) The detailed binding pose of TBC in site J. (c) The detailed binding pose of CBD in site J. (d) The comparisons of residue energy contribution of the binding residues for these AMs in site J. 30

Figure 8. The time course of root–mean–square deviations (RMSD) of mainchain atoms of the transmembrane domains (7TM, black), heavy atoms of CP55940 after least-square (LS) fitting (9GF, red) and heavy atoms of CP55940 without fitting (9GF, green). To calculate the No-Fit RMSDs for CP55940, the mainchain atoms of 7TM were first aligned and the resulting translation–rotation matrix were then applied to the ligand. After the coordinate transformation, the RMSDs were calculated directly. (A) CP55940/CB2 without C-2 binding, (B) site B, (C) site G, (D) site H, (E) site I and (F) site J. 31

Figure 9. The time course of root–mean–square deviations of mainchain atoms of the transmembrane domains (7TM, black), heavy atoms of C-2 after least-square (LS) fitting (LIG, red) and heavy atoms of C-2 without fitting (LIG, green). To calculate the No-Fit RMSDs for C-2, the mainchain atoms of 7TM were first aligned and the resulting translation–rotation matrix were then applied to the ligand. After the coordinate transformation, the RMSDs were calculated directly. (A) site B, (B) site G, (C) site H, (D) site I and (E) site J. 32

Figure 10. The detailed interactions between C-2, CP55940, and CB2 receptor where C-2 resides in site H. (A) The crystal structure of CP55940/CB2 with C-2, the PAM binding at site H. (B) The CB2 residues surrounding CP55940 and C-2. (C) The representative MD structure (the one that is structurally most similar to the average structure). (D) The residues surrounding CP55940 and C-2 in the representative MD structure. Two hydrogen bonds are formed between C-2 and CB2 residues (H95$^{2.65}$, and K278$^{7.31}$), and two hydrogen bond is formed between CP55940 and CB2 residues (S285$^{7.38}$ and L182). The hydrogen bonds are shown as magenta dashed lines. 37

List of Equations

Equation 1 Five core terms (gauss1, gauss2, repulsion, hydrophobic, and hbonding) used by scoring function in MCCS..... 13

Equation 2 The total score formed by the weighted sum of the five core terms..... 13

Equation 3 The residue energy contribution calculated by MCCS scoring function..... 13

Preface

I first would like to appreciate my advisor Dr. Zhiwei Feng, who is the world outstanding expert in the computer-aided drug design and algorithm development. I appreciate Dr. Feng's guidance in these two years for teaching me so many computational techniques as well as his help in both my study and life. In our weekly group meeting, I never forget my exciting feeling when Dr. Feng introduced a new software or new algorithm to us. Because of that, I gradually got to know the whole workflow of computer-aided drug design and became familiar with various computational techniques and software. Thanks to Dr. Feng, I gradually became interested in working in dry lab and realized its important role in the drug development process. Besides the relationship as advisor and student, we are good friends with each other.

I would also like to thank Dr. Kirisci, an expert in both mathematical and applied statistics, who taught me Statistical Methods during the first semester. His clear and logistic teaching method helps me to learn many useful data processing and analyzing approaches. And what he taught inspired me a lot in my study and research.

During the two-year research experience, I like the teamwork and the harmonious, positive atmosphere in our lab as well as the whole PSP track. I'm impressed about our program's dedication to the area of developing therapeutics, the cutting-edge research topics,

the completed, systematic experimental and theoretical training through multidisciplinary communication. Dr. Wang gave me great support on conducting MD simulations on my research. I appreciate his patience and careful introduction to the mechanism and the data processing approaches. I am also so glad to meet with Dr. McGuire, who is so nice and friendly. I still remember my embarrassment during the first and second presentations in the CB2 RO1 meeting. It was Dr. McGuire who always encouraged and praised me, giving me such great confidence in my work. Although Dr. Xie is busy, when I have problems with my research and study, he was always here to give me suggestions and help me to release stress. I admire Dr. Jun's rigorous and serious attitude towards research. He helped me a lot when I was working on the review.

Except for faculties, I would like to say thanks to my lovely colleagues. Chen Jiang, Chih-Jung Chen, Yixuan Hao, and Bo Yang gave me great help on my research. Thanks to their contributions, I could have my first-author paper and review finished and published on time. And I appreciated Chen Jiang, Yixuan Hao, He Zhang, Yuchen Sun, Jingming Cao, and Tianqi Wang who are close friends in my life. I am not a person who is very good at taking care of myself in life, thanks to my lovely friends taking care of me and their companionship. That makes me feel at home. I would also like to give my appreciation to the senior students I met during my MS school life. They are so patient and so nice to unreservedly tell me their experience and knowledge on both study and life, which help me take fewer detours. It's my fortune to have this opportunity to know and become friends with all of you. The time I spent with you guys is the most precious time when I'm abroad, which is worthy for me to remember for my entire life.

Most importantly, I love my dear family and boyfriend. Thanks for encouraging me, trusting me, sharing the happiness and tears with me. You are always my strongest backing and the people I care about most. Hope you are all in good health. Miss you.

At last, thanks for PSP track, CCGS center, school of Pharmacy, the University of Pittsburgh that provide me a great platform to foster my growth, get me closer to my career goal, and help me realize my aspiration to devote myself to the human health development in the future.

1.0 Instruction

1.1 The Human Endocannabinoid System (ECS)

The endocannabinoid system (ECS) is a lipid signaling system [1] that consists of cannabinoid receptors, enzymes, and endocannabinoids expressed in the major domain of the mesocorticolimbic system [2]. It not only plays a vital role in multiple physiological processes but also acts as a valuable therapeutic target to be validated and developed for treating neurodegenerative diseases [3], autoimmune diseases, inflammatory diseases, psychosis, mood disorders [4], pain [5], as well as for modulating the smooth muscle motility [6] and the gut integrity in the gastrointestinal tract [7]. Besides these positive implications, ECS is also involved in reward processing as well as drug addiction [8]. Therefore, ECS drugs should be developed to balance the therapeutic effects and adverse events.

So far, CB1 and CB2 are the most abundant receptors in the ECS, classified as canonical CB receptors and belonging to G protein-coupled receptors [9]. Orphan GPCRs, such as GPR55 [10] and GPR18 [11], ionotropic receptors like transient receptor potential channels [12], nuclear receptors including peroxisome proliferator-activated receptors [13], as well as ligand-based ion channels, such as nicotinic acetylcholine [14] and $GABA_A$ receptors [15] are also related to the endocannabinoid system. Here, we mainly focus on CB1 and CB2 receptors.

1.2 Cannabinoid Receptor 1 and Cannabinoid Receptor 2

1.2.1 Distribution and Therapeutic Effects

CB1 makes up the majority of G protein-coupled receptor in the central nervous system (CNS). It is highly expressed in the basal ganglia nuclei, the cortex, the hippocampus, the olfactory system, the hypothalamus as well as cerebellum [16]. CB1 expression also appears in some peripheral nervous systems, for example, in sensory neuron synaptic terminals [17]. Due to its wide distribution in the CNS, CB1 receptors are targeted to mediate pain and inflammation, as well as treat psychotropic effects [18]. However, synthetic cannabinoids that target CB1 may cause serious side effects, including drug dependence, memory impairment as well as convulsions, and so on [19]. CB2 is mainly expressed in the periphery immune system, especially blood cells [18], macrophages, thymus, leukocytes and so on [19] with limited expression in the CNS [9]. The essential role of CB2 receptors in therapeutics is participating in the treatment of neurodegenerative diseases, autoimmune diseases, osteoporosis, and more [20-22]. Activated CB2 receptors can work together to reduce the immune response, preventing the over-inflammation through both the immune and neuronal pathways [23]. Most importantly, they have the potential to regulate addition and dependence disorders [24]. Taking the distribution of CB1 and CB2 into consideration, ECS drugs selectively targeting CB2 could help to avoid the CNS adverse effects.

1.2.2 Structural Information

Both the CB1 and CB2 receptors have seven transmembranes (TMs) alpha-helices connected by three intracellular loops (ICLs) and three extracellular loops (ECLs), which form the

C-terminal domain and N-terminal domain, respectively, as well as one amphipathic helix [25, 26]. They share a tremendous total sequence identity of 42-44% [27], and they have 68% sequence similarity in the TM regions [19]. When orthosteric ligands bind to the receptors, it has been reported that the structural conformation of the CB2-antagonist AM10257 complex is more constrained than that of the CB1-antagonist AM6538 complex. Interestingly, the CB2-antagonist AM10257 not only has closely resembled structural conformation but has almost the same orthosteric binding pocket of CB1-agonist AM11542, including size as well as ligand-interacting residues [26]. Besides, Xing et.al also obtained the cryo-EM structure of the CB2-Gi signaling complex coupled with agonist WIN 55,212-2 revealed to occupy the same orthosteric pocket as antagonist AM10257 [25]. Meanwhile, both the X-ray crystal and cryo-EM structures of CB1-orthosteric agonist AM841-Gi protein-scfv16 complex demonstrated a high degree of similarity to the complex of CB2-orthosteric agonist AM12033-Gi protein-scfv16 (RMSD=1.65 angstrom). They have superimposable binding poses of orthosteric ligands, and even the surrounding residues have similar confirmations [28]. The structural information of CB1-agonist, CB1-antagonist, CB2-antagonist, and CB2-agonist facilitates ECS research and promotes the development of their relative drugs.

The different states could also influence the structures of the receptors. When cannabinoid receptors change from an inactive state to an active state, CB1 suffers from a considerable conformational change in both ECLs and ICLs, while the ECLs and N terminus of CB2 change minorly [28].

1.3 Orthosteric Ligands and Allosteric Modulators

1.3.1 Classification

Orthosteric ligands of the ECS can be endogenous or plant-derived, like phytocannabinoids, or synthetic compounds that act as an agonist, antagonist, or inverse agonist [29]. They directly bind to CB1 or CB2 receptors in their orthosteric binding sites then affect downstream signaling pathways. For example, WIN55,212-2 and CP55940 are two non-selective agonists of CB1 and CB2. Allosteric modulators (AMs) bind to another region of the receptors and regulate the response triggered by orthosteric ligands. AMs classify into four groups: positive allosteric modulators (PAMs) and negative allosteric modulators (NAMs), which can activate or inhibit the receptor response, respectively, and silent or neural allosteric modulators, that bind to allosteric without affecting agonist response. Another group is bitopic ligands, binding to both orthosteric and allosteric sites [30], for example, agonist-positive allosteric modulator (ago-PAM) [31, 32], can activate an intracellular signaling response without an orthosteric agonist. One of the possible mechanisms of how PAM or NAM regulate orthosteric responses is that PAM/ NAM can bind to the extracellular regions of the receptors, then stabilize/induce their active states. The other is that small molecules or even peptides can bind to the intracellular regions of the receptors and hinder the detailed interactions between proteins [33].

1.3.2 Development

To date, many orthosteric ligands of CB1 and CB2 are in circulation while the number of AMs is still limited, especially for CB2 receptors. Since the main constituents of Cannabis got

successfully isolated in the 1960s, 9-tetrahydrocannabinol (Δ9-THC) and cannabinoid (CBD) started the earliest discovery of ECS ligands [34]. However, due to the multi-directional nature of ECS [35], several synthetic molecules with serious adverse events were developed. The most notorious one is Rimonabant: an anti-obesity drug that acted as a CB1 inverse agonist was first approved in 2006 but then withdrawn in 2008 due to several psychiatric effects, like anxiety, depression, and suicidal tendencies [36]. Until 2017, only four drugs targeted on cannabinoid receptors have been approved by the FDA. 17 drug candidates targeted on CB1 and nine targeted on CB2 are in clinical trials. All these molecules are orthosteric ligands, except namacizumab, a NAM of CB1 receptor, and are still ongoing in clinical trials [37-39]. CB receptors also belong to Class A GPCRs. Nowadays, more and more AMs of GPCRs have been discovered as potential drugs [40]. For example, Ticagrelor is an anti-thrombosis drug approved by FDA, which acts as an allosteric antagonist and targets on P2Y receptor [41]. Maraviroc is a NAM of CC chemokine receptor type 5 (CCR5), which is approved for the treatment of HIV infection [42]. Another example is Plerixafor, a NAM of CXC chemokine receptor type 4 (CXCR4), approved by the FDA for the treatment of bone marrow transplantation [33, 43].

1.4 Downstream signaling pathways

After binding with ligands, activated cannabinoid receptors can elicit a complex matrix of intracellular effects via different signaling pathways, including G-proteins and beta-arrestins [44]. G-proteins modulate the stimulated adenylyl cyclase (cAMP). The recruitment of beta-arrestins can inhibit the G-proteins coupling and quenching the G-proteins signals and increase the tolerance of repeated stimulation, also known as desensitization [9, 45]. Active CB1 mainly couples to Gi/o

protein to reduce cAMP level, inhibiting the release of the pre-synaptic neurotransmitters. Through the G-protein-dependent pathway as well as the beta-arrestin pathway, it also improves the phosphorylation of extracellular signal-regulated kinase ½ (pERK1/2). It activates the mitogen-activated protein kinase (MAPK) to modulate nuclear transcription. It has been reported that CB1 can also couple with Gs and Gq/11 proteins to instigate cAMP levels [28, 46-48]. While as for CB2, couples to Gi/o protein to inhibit cAMP signals [25], activates ERK1/2 kinases, modulates the MAP kinases pathway [49-51]. Activated cannabinoid receptors (CBRs) can also initiate a transient Ca2+ signaling elevation in the endothelial cells which is probe-dependent [52, 53]. But CB2 has little interaction with Gs and Gq/11 proteins. Thus, a ligand that selectively evokes a specific downstream signaling pathway could be a better choice for therapeutics.

1.5 Endocannabinoids (eCBs)

Endocannabinoids (eCBs) are endogenous lipid messengers which participate in various physiological processes [2] and are synthesized or degraded by relative enzymes, including fatty acid amide hydrolase (FAAH) and monoacylglycerol lipase (MAGL) [54-56]. Both Anandamide (AEA) and 2-arachidonoylglycerol (2-AG) are derivatives of arachidonic acid [57, 58]. AEA is the most abundant endocannabinoid in the human body, a partial agonist of the CB1 receptor, and is almost inactive in the CB2 receptor. And CB1 coupled with AEA has no signaling bias [59]. Besides, 2-AG is 170-fold more abundant than AEA in the brain. It is a full agonist of CB1 and CB2 receptors with different affinities. CB2 coupled with 2-AG is biased on the beta-arrestin pathway [9, 59]. Thus, for one receptor, different orthosteric ligands may produce different signaling responses in the same receptor.

1.6 Advantages and Disadvantages of AMs

As we mentioned above, few FDA-approved drugs that target CB1 or CB2 are on the market, and they are all orthosteric molecules. Moreso, many of them in clinical trials have been abandoned [33]. That is because their nonspecific binding to other homologous receptors that have highly conversed orthosteric binding sites produces serious off-target adverse effects [4, 60, 61]. To overcome this problem, AMs present as a choice with several important advantages. First, more excellent receptor subtype selectivity. AMs bind to allosteric binding sites with lower evolutionary conservation, reducing off-target side effects. Besides, allosteric effects depend on orthosteric ligands (probe-dependence). AMs generate effects with only the presence of orthosteric ligands (except ago-PAM) without introducing competition and regulate the biased signaling pathways caused by orthosteric ligands through inducing or stabilizing the conformations of the receptor. Then, saturability. When the concentration of AMs increases to a certain degree, adding more AMs cannot change the orthosteric response, which decreases or avoids a drug overdose. The combination of probe dependence and signaling bias has the potential to allow a more optimized and precise pharmaceutical regulation of specific signaling pathways, providing a promising direction for ECS drug development and design [22, 49, 62-64].

1.7 Aims and work

We recently summarized 11 PDB files [65] containing the crystal structures of reported Class A GPCRs (including Alpha, Delta, and Gamma sub-branches). We also discussed the reported allosteric binding sites in this study and found that four allosteric binding sites are more

typical than others. Meanwhile, due to the limited number of reported crystal structures of receptor–AM, the conclusion for each allosteric binding site may only indicate the possible binding features of the receptor–AM complex.

As we know, the structure of CB1 is the most similar to that of CB2 among GPCRs. There are seven X-ray crystal or cryo-EM structures of CB1 in the Protein Data Bank (RCSB PDB: Homepage accessed on 01 January 2022). Among them, one complex of CB1-agonist-NAM has been reported. In the crystal structure of CB1-CP55940-ORG27569 [66], ORG27569 is a NAM of CB1 and CP55940 is an orthosteric agonist of CBs (refers to CB1 and CB2) [66]. Meanwhile, only four complexes of CB2 are available, including two complexes of CB2-agonist [28], a 3D cryo-EM structure of CB2-WIN 55,212-2-Gi signaling complex [25], and a structure of CB2 coupled with antagonist [26]. In addition, several AMs have been discovered for CB2, including pepcan-12 [67], compound Ec2la (C-2) [30], trans-β-caryophyllene (TBC) [68] and cannabidiol (CBD) [68]. However, we still do not know how these AMs bind to CB2, and there is no X-ray crystal or cryo-EM structure of CB2-orthosteric ligand(s) coupled with the modulator. All the missing information seriously hinders the drug discovery and development process of CB2 allosteric modulators.

In the present work, we mainly focused on investigating the potential allosteric binding site(s) of CB2. We first predicted the allosteric cavities of CB2 in the presence of CP55940 or WIN 55,212-2 using three different algorithms. We then docked three reported AMs into each predicted site of CB2 and analyzed the detailed interactions and energy distribution between AMs and involved residues. By selecting the binding pose of C-2 with the lowest total energy contribution in each allosteric site, we sequentially carried out the MD simulations for the

complexes of CB2-CP55940-C-2 coupled with Gi protein. Based on our findings, we suggest that site H is the most promising allosteric binding site of C-2[69].

2.0 Materials and Methods

2.1 3D structures of CB2

The cryo-EM structure of CB2 coupled with agonist-WIN 55,212-2 [70] was collected from the Protein Data Bank (https://www.rcsb.org/ accessed on 1 January 2022) [71, 72]. Since there is no available crystal or cryo-EM structure of CB2-CP55940, we built this complex using the molecular docking approach. CP55940 is a non-selective agonist of CB1 and CB2 [73]. The crystal 3D structure of CB1-CP55940 [66] was used to select the most appropriate binding pose of CP55940 in CB2[69]. In the modeled CB2-CP55940 complex, CP55940 has the same binding pose as that in CB2-CP55940 with the highest docking score.

2.2 Predictions of Allosteric Binding Sites of CB2

Three algorithms or software were used to predict the potential allosteric binding sites of CB2, including the CavityPlus (http://www.pkumdl.cn:8000/cavityplus/index.php accessed on 01 J accessed on 01 January 2022) [74], and Sybyl-X 1.3 (SYBYL-X Software | Certara)[69].

In CavityPlus, we adopted the Cavity module and CorrSite 2.0 submodule. First, we upload the CB2 structure of PDB:6PT0 by removing WIN55,212-2. Based on the structural geometry-based method, the Cavity module can detect the potential binding sites on a given protein structure, which were then ranked by their ligandability and druggability quantitatively assessed by CavityScore and CavityDrugScore respectively. Next, CorrSite 2.0 is adopted to further identify

the allosteric sites with higher potentiality among all the predicted cavities. We defined the orthosteric sites by uploading a custom pocket generated by PDB:6PT0 via selecting the residues within 4.0 angstroms. Based on the hypothesis that there was a high correlation between the motions of orthosteric and allosteric sites, CorrSite 2.0 calculates the motion correlation between the allosteric binding sites and the known orthosteric binding site. We selected the sites with a z-score higher than 0.5[69].

In PARS, we uploaded the complex of CB2-CP55940/CB2-WIN55,212-2 and the potential binding sites were generated with overall flexibility value and structural conservation.

In Sybyl-X, we adopted the Surflex-Dock module, uploaded the complex of CB2-CP55940/CB2-WIN55,212-2, and defined the binding sites with multi-channel surface mode. We set “Threshold” as 0.50 and “Bloat” as 0.

Then, we aligned the pockets generated by three algorithms and tools, selected the binding sites detected in all two complexes by at least two methods, and compared them to the X-ray crystal and cryo-EM structures of GPCRs[69].

2.3 Molecular Complex Characterizing System (MCCS)

Here we applied MCCS [75] to prepare the complexes and calculate the residue energy contribution. Firstly, each PDB was divided into two parts: an orthosteric ligand PDB and a protein PDB. A protein PDB may contain both a protein and an allosteric modulator, or just the protein structure. Chimera (version 1.15) [76] was used to fix residues with an incomplete side chain in protein PDBs. Specifically, Chimera scanned the full protein structures at first, then revealed the uncompleted residues. Using the Dunbrack rotamer library, the truncated side chains were replaced

with a whole side chain of the same residue type [77]. The polar hydrogens, Vina force field, and Gasteiger charges were then added using VEGA [78]. Finally, the PDB protein format was converted to PDBQT. For ligand files, the VEGA was first used to prepare ligand PDBs for the same reason as the protein preparation. The pKa values of ligands were then predicted using PROPKA (version 3.1) [79, 80]. MCCS would protonate the tertiary (3°) amide in the compounds when the computed pKa value of the ligands was greater than or equal to the supplied pH (7.4 by default). Finally, the torsions of ligands were determined by VEGA, and the ligand file format was changed from PDB to PDBQT. The PDBQT files of protein and ligand, as well as the pKa file of the ligand, were used as input for the following phase in MCCS, which is scoring and docking with jdock (version 2.2.3b, GitHub - stcmz/jdock: An extended variant of idock which was originally developed by @HongjianLi. accessed on 01 January 2022) [75] to prepare the complexes and to calculate the residue energy contribution[69].

Jdock is a core implementation of MCCS and is a version and successor of idock [81]. jdock can generate a vector of residue-free energy from the conformation predicted by a Monte Carlo-based docking algorithm or determined by X-ray crystallography or cryo-EM by using the same five-term scoring function (gauss1, gauss2, repulsion, hydrophobic, and h-bonding) invented by AutoDock Vina [82, 83]. There are three modes: “docking” mode, “score only” mode, and “scoring & docking” mode. For a given receptor complex, the scoring function can generate nine binding recognition vectors: (1) Gauss (Gauss1 + Gauss2), (2) Gauss1, (3) Gauss2, (4) repulsion, (5) steric (Gauss1 + Gauss2 + repulsion), (6) hydrogen-bonding, (7) hydrophobic, (8) non-steric (hydrogen-bonding + hydrophobic) and (9) residue energy contribution. Below are the fire core terms used by the scoring function in MCCS which is shown in Equation 1 (“dij” is a variable that represents the surface distance between the interacting atoms) [75]:

$$gauss1\ (dij) = e^{-(\frac{dij}{0.5})^2} \quad (1)$$

$$gauss2\ (dij) = e^{-(\frac{dij-3}{2})^2} \quad (2)$$

$$repulsion\ (dij) = \begin{cases} dij^2,\ if\ dij < 0 \\ 0,\ if\ dij \geq 0 \end{cases} \quad (3)$$

$$hydrophobic\ (dij) = \begin{cases} 1,\ if\ hydrophobic\ and\ dij \leq 0.5 \\ 1.5 - dij,\ if\ hydrophobic\ and\ 0.5 < dij < 1.5 \\ 0,\ if\ not\ hydrophobic\ or\ dij \geq 1.5 \end{cases} \quad (4)$$

$$hbonding\ (dij) = \begin{cases} 1,\ if\ hbonding\ and\ dij \leq -0.7 \\ \frac{dij}{-0.7},\ if\ hbonding\ and\ -0.7 < dij < 0 \\ 0,\ if\ not\ hbonding\ or\ dij \geq 0 \end{cases} \quad (5)$$

Equation 1 Five core terms (gauss1, gauss2, repulsion, hydrophobic, and hbonding) used by scoring function in MCCS

The weighted sum of the five terms forms the total score, where the coefficients are also given in the original Vina literature [75]:

$$\begin{aligned} score_{atom}(dij) &= (-0.035579) \times gauss1(dij) + (-0.005156) \times gauss2(dij) \\ &+ (+0.840245) \times repulsion(dij) + (-0.035069) \times hydrophobic(dij) \\ &+ (-0.587439) \times hbonding(dij) \end{aligned}$$

Equation 2 The total score formed by the weighted sum of the five core terms

The residue energy contribution is calculated as:

$$score_{residue}(R, L) = \sum_{\substack{i \in R \\ i \in L}} score_{atom}(dij)$$

Equation 3 The residue energy contribution calculated by MCCS scoring function

Here, R is the set of atoms in the residue being considered and L is the set of atoms in the ligand whose coordinates are either computed from Monte Carlo based docking or determined by X-ray crystallography or cryo-EM [75]. Other information about MCCS is available in our previous literature [75].

A maximum of 999 binding poses can be generated by the docking mechanism in jdock-ligand. The X-ray crystal and cryo-EM structures were computed in "score only" mode, in which the scores of all receptor-ligand atom pairs were directly calculated and added to the overall score [69]. We used the 'scoring & docking' function to find the most promising binding pose of AM and analyze the detailed interactions of AM in each site via the modeled CB2-CP55940 complex. We also used the 'scoring' function to analyze the residue energy contribution of the 3D structures of Class A GPCRs.

2.4 Molecular Dynamics (MD) Simulation

Five complexes of CB2-CP55940-C-2 coupled with Gi proteins were used to perform the MD simulations, in which C-2 bound to five predicted allosteric sites. The system without C-2 binding was also prepared as a control to investigate if C-2 can enhance or decrease CP-55940 binding. Each system was put into a 0.15M NaCl solution with a cubic water box and 240 POPC lipid molecules and about 63891 TIP3P [84] water molecules. Charmmgui (https://charmm-gui.org accessed on 01 January 2022) Online Toolkit was applied to add POPC lipids. The protein, lipid, and small molecules were modeled using FF14SB [85], lipid14 [86, 87], force fields, respectively. All MD simulations were performed using the AMBER 18 software package [69, 88].

Each MD system was first relaxed by five 10000-step minimizations followed by five restrained MD simulations to remove possible steric clashes. Each restrained MD simulation lasted 1 nanosecond (ns). using an integration time step of 1 femtosecond (fs). The five minimization and restrained MD runs applied 20, 10, 5, 1, and 0 kcal/mol to the mainchain atoms, sequentially. After the system was relaxed, three NPT (constant particle number, pressure, and temperature) MD simulation phases were conducted sequentially: the heating-up phase (2 ns for each temperature from 50 to 250 K at a step of 50 K); the equilibrium phase (12 ns, 298 K); and the sampling phase (125 ns). The integration of the equations of motion was conducted at a time step of 2 fs for all three phases. Other MD protocols were detailed in the previous publication [69, 89].

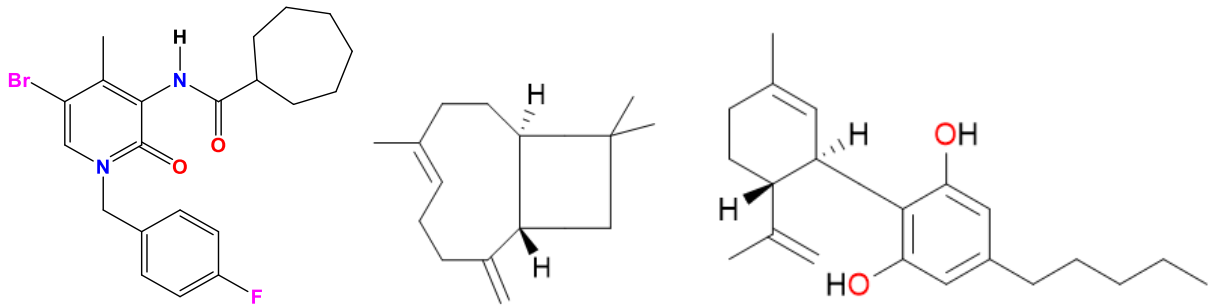

Figure 1 CB2R AM: C-2 (left), TBC (middle), and CBD (right)

2.5 Post-MD analysis

The post-MD analysis we chose was Molecular Mechanics/Generalized Born Surface Area (MM/GBSA) Calculation. 250 MD snapshots were evenly selected from the sampling phase for the MM-PBSA-WSAS free energy calculations. For each MD snapshot, the molecular mechanical (MM) energy (EMM) and the Poisson–Boltzmann Surface Area (PBSA) energy terms were calculated without further minimization. Unlike the common MM-PBSA protocol for non-

membrane proteins, two external dielectrics (ewat = 80 for water and elip = 1.0 for the lipid bilayer) were applied for our systems. The membrane center offset parameter (mctrdz) was calculated for an individual snapshot using the coordinate centers of the CB2 receptor and the POPC bilayer. Similarly, the thickness of the membrane for an individual snapshot was calculated as the distance between the centers of phosphorus atoms in the upper and lower layers of the lipids. For ligands CP55940 and C-2 themselves, the implicit membrane option was turned off and the external dielectric constant was set to 80. The nonpolar solvation energies were estimated by multiplying the solvent-accessible surface areas (SAS) with surface tension coefficient plus a constant. In this work, surface tension and constant are 0.0054 kcal/(mol·$Å^2$) and 0.92 kcal/mol, respectively. Note that an efficient model, WSAS, was applied to calculate the entropy contribution (TS) [90]. For MM-PBSA-WSAS binding free energy calculations, a single-trajectory protocol was applied [91], i.e., only the MD trajectories of the complex were sampled, and the receptor and ligand coordinates were extracted from the complex ones. Using this protocol, the internal energies do not contribute to the ligand binding, with a return of good error cancellation. However, in MM-PBSA-WSAS free energy calculation for the complexes, the internal energy terms (E_{int}) as well as the 1–4 electrostatic (E_{ele}) and van der Waals (E_{VDW}) terms were all included[69].

3.0 Results

3.1 Overview of Seven Predicted Allosteric Binding Sites of CB2

Three different algorithms including CavityPlus, Protein Allosteric and Regulatory Sites (PARS), and Sybyl-X were used to predict the potential allosteric binding sites of CB2 using both the cryo-EM structure of CB2-WIN 55,212-2 [25] and the modeled complex of CB2-CP55940 [66, 69].

As shown in Figure 1, there were a total of seven promising allosteric binding sites predicted by the algorithms. Among them, four allosteric sites were supported by the reported allosteric binding pockets in Class A GPCRs, including sites B, C, G, and K[69].

Site B is located between the TM3 and TM4 and is close to the intracellular loop 2 (ICL2), which is supported by two 3D structures, including the complex of beta-2 adrenergic receptor (ADRB2)-orthosteric agonist BI167107-PAM Compound-6FA (Cmpd-6FA) reported by Liu and co-workers [92] (PDB:6N48), and the complex of free fatty acid human receptor 1 GPR40 (FFAR1)-orthosteric partial agonist MK-8666-PAM compound-AP8 (Cmpd-AP8, PDB:5TZY). After aligning those two crystal structures with the CB2 receptor, we found that Cmpd-6FA locates exactly at the same position as site B. The carboxylate group of Cmpd-AP8 inserts in a polar cavity of FFAR1 formed by TM3, TM4, and ICL2, which is the same position as site B in Figure 1 [93]. Recently, the cryo-EM structures of dopamine D1 receptor (DRD1)-orthosteric agonist dopamine-PAM LY3154207 (PDB: 7CKZ) has been reported by Xiao and co-workers. The binding site of LY3154207 is created by ICL2, TM3 as well as TM4, which is also the same position as site B [69, 94].

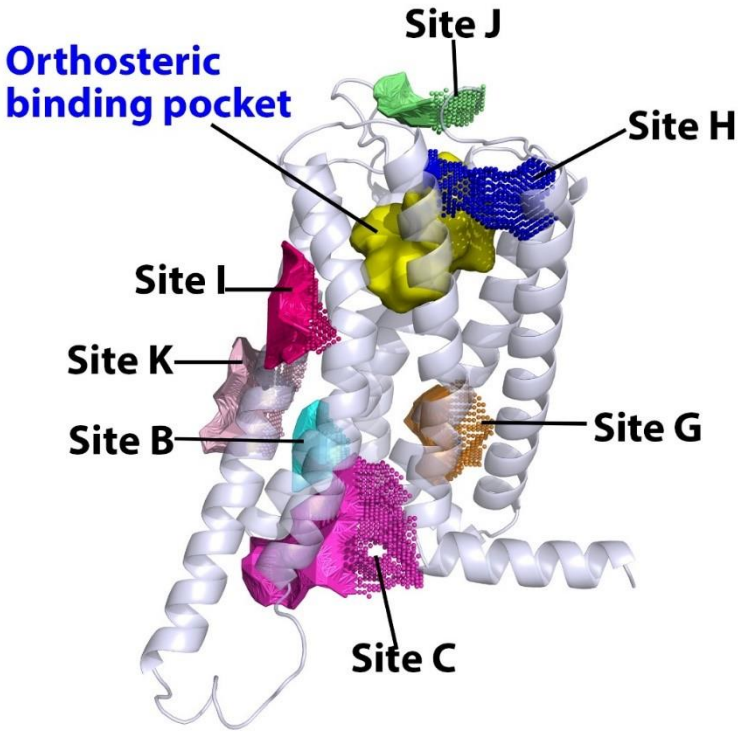

Figure 2. Predicted allosteric binding sites of CB2 by CavityPlus, Protein Allosteric and Regulatory Sites (PARS), and Sybyl-X. The orthosteric binding site was highlighted in yellow surface, while predicted allosteric sites are highlighted in dots.

Site C is located within the receptor's helical bundle, TMs 1-3, TMs 6-7, and helix 8, on the intracellular side of the CB2 receptor. It is accessible from the cytoplasm, and it overlaps with the Gα binding site. This site is supported by the crystal structure (PDB:5T1A) of CC chemokine receptor type 2 (CCR2)-orthosteric antagonist BMS-681-NAM CCR2-RA-[R] published by Zheng and colleagues [95]. The position of site C has also been demonstrated by other crystal structures of CC chemokine receptor type 9 (CCR9)-NAM vereirnon (PDB:5LWE) [96] as well as the complex of ADRB2-orthosteric antagonist Carazolol-NAM Compound-15PA (Cmpd-15PA) (PDB:5X7D) [97]. All these NAMs mentioned above locate at the intracellular site of their

receptors and appeared to sterically interfere with the G-protein binding to their receptors [69, 95-97].

Moreover, site G is at the extrahelical site in the inner part of the membrane, which is located at the bottom of TMs 1, 2, 3, and 4. Site G is supported by the crystal structure of CB1-orthosteric antagonist CP55940-NAM ORG27569 (PDB:6KQI) [66, 69].

The location of site K between TM3 and TM5 is supported by the 3D structure of ADRB2-orthosteric antagonist alprenolol-NAM AS408 (PDB:6OBA). They found that the well-defined Fo–Fc electron densities for AS408 are on the membrane-facing surfaces of TM3 and TM5, but not in the extracellular vestibule [98]. Another supporting 3D structure of site K is C5a anaphylatoxin chemotactic receptor 1 (C5aR1)-NAM NDT9513727 (PDB:5O9H) [99]. By aligning the crystal structure of the C5aR1 human receptor with the ADRB2 structure (PDB:6OBA), we observed that NDT9513727 binds to the same region as the location of NAM-AS408 in the ADRB2 human receptor, which is consistent with the site K in Figure 1[69].

For the other three novel allosteric binding sites, site J is located at the top of TMs 3-7, site I is near TMs 5 and 6, while site H is close to the orthosteric binding site that formed by the residues in TMs 1, 2 and 7. The promising binding residues involved in these potential allosteric binding sites will be discussed in the following sections[69].

3.2 Detailed Binding Poses and Interactions of AMs in Site B, K, and C of CB2

Up to date, C-2 (PAM) [30], TBC (NAM) [100] and CBD (NAM) [68] are the reported CB2 small-molecule AMs. As shown in Table 1, we first docked these three AMs into seven predicted allosteric sites of the CB2 in the presence of agonist-CP55940. The binding pose of

CP55940 in CB2 was identical to that in CB1. We also scored the crystal structures of other GPCRs that supported our predicted binding site and made comparisons with the detailed residue energy contribution of CB2[69].

Table 1. The comparisons of docking scores of AMs in various allosteric binding sites(kcal/mol).

	Site B	Site C	Site G	Site H	Site I	Site J	Site K
C-2	-5.59	N/A*	-6.34	-4.31	-7.34	-5.75	-7.23
TBC	-6.04	-4.44	-5.42	-2.79	-6.39	-4.35	-5.75
CBD	-6.28	-4.74	-5.89	-4.21	-5.92	-4.13	-5.78

* N/A: based on the reported crystal structures, we suggested C-2 (PAM) did not bind to site C.

As shown in Figure 2, we docked C-2 into site B, TBC/CBD into site C, and all three AMs into site K. Especially, C-2 formed a hydrogen bond with $T153^{4.45}$ and steric interactions with $I129^{3.48}$, and $R149^{4.41}$ in site B. $I129^{3.48}$ also forms strong hydrophobic interaction with C-2. These important residues involved in the binding of C-2 were supported by the crystal structures of the human FFAR1 receptor and human ADRB2 receptor [92, 93]. In our scoring results, Cmpd-6FA, a PAM locates in site B of ADRB2, interacts with $F133^{3.52}$ and $L144^{ICL2}$ via hydrophobic and steric interactions and forms a strong hydrogen bond with $K149^{4.41}$, which are consistent with the literature [92]. To study the detailed interaction of AMs in site B, we also docked TBC/CBD into site B. We found that $I129^{3.48}$, $L145^{ICL2}$, $R149^{4.41,}$ and $T153^{4.45}$ were the residues with high energy contribution for TBC and CBD. However, in the detailed energy contribution of C-2, although $L145^{ICL2}$ contributes much total energy to the binding of C-2, it does not form strong interaction. Both arginine and lysine were basic residues with positively charged side chains, so the

interactions between K149$^{4.41}$ (ADRB2) and AMs were similar to that of R149$^{4.41}$ (CB2). We predicted that T153$^{4.45}$, I129$^{3.48}$, and R149$^{4.41}$ are potential key residues in site B[69].

In site C, TBC formed the steric interactions with R131$^{3.50}$, R302$^{7.56}$, Y70$^{2.40,}$ and S303$^{8.47}$, while CBD formed hydrogen bonds with Y70$^{2.40}$, R131$^{3.50,}$ and S303$^{8.47}$. The key residues for the binding of TBC and CBD are supported by the crystal structures of the CCR2 human receptor, CCR9 human receptor, and ADRB2 human receptor [95-97]. For example, Cmpd-15PA, a NAM of ADRB2, forms hydrogen bonds with R63^{ICL1}, D331$^{8.49}$, S329$^{8.47,}$ and T274$^{6.36}$ and hydrophobic interactions with Y326$^{7.53}$, F332$^{8.50,}$ and L64^{ICL1}. We found that at position 8.47, serine was the only overlapped residue that formed the same interaction between CB2 and ADRB2. However, the binding poses of NAMs in CCR9, CCR2, and ADRB2 were much closer to TMs 1, 7, and helix 8 compared to the binding poses of TBC/CBD in CB2 due to the spatial block by Y70$^{2.40}$. Taking all the supporting literature and the binding site of Gi protein into consideration, we inferred that C-2 (PAM) was less possible to bind at site C[69].

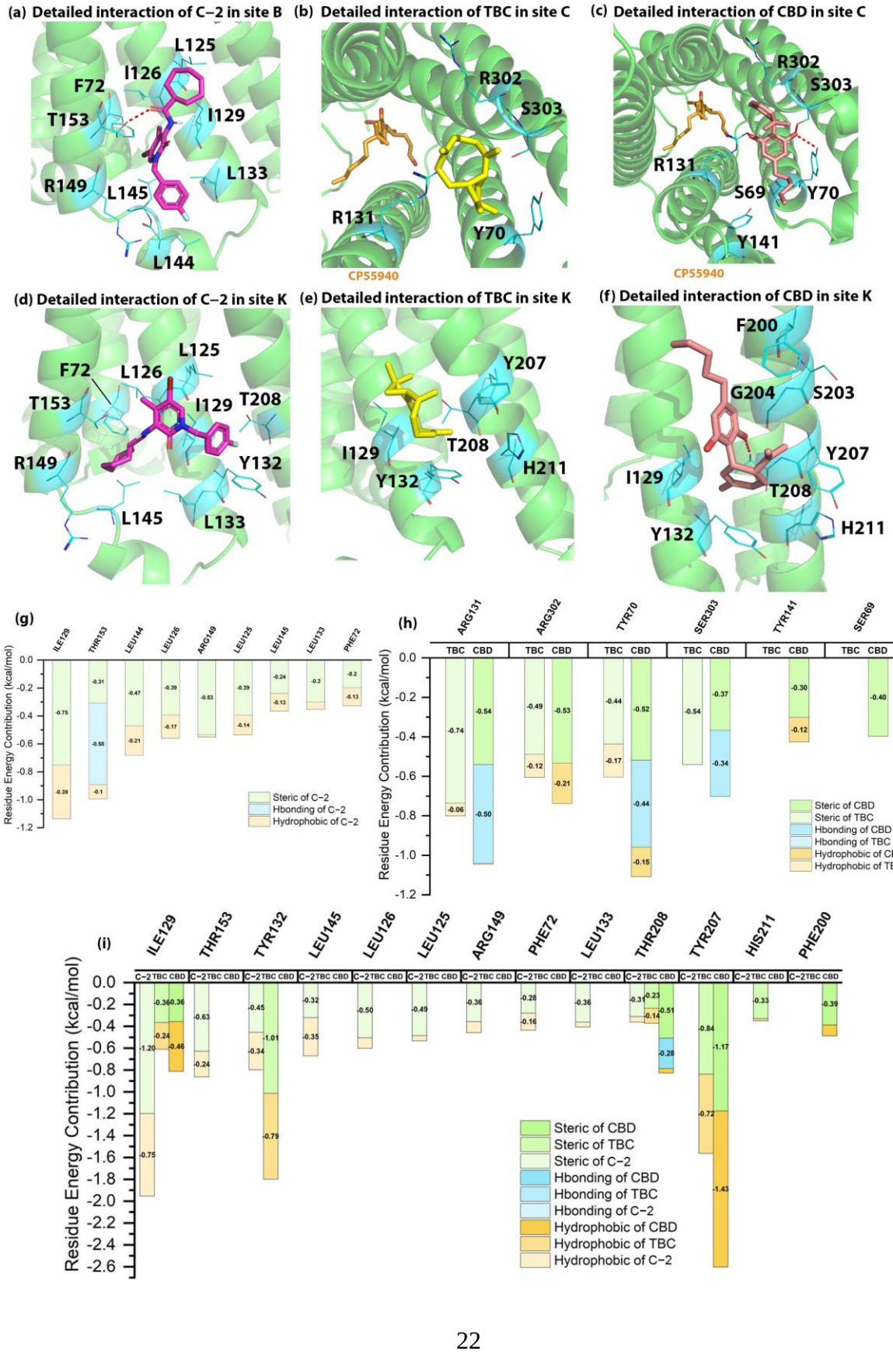
(a) Detailed interaction of C−2 in site B
L125
I126
F72
T153
I129
L133
R149
L145
L144
(b) Detailed interaction of TBC in site C
R302
S303
R131
Y70
CP55940
(c) Detailed interaction of CBD in site C
R302
S303
R131
S69
Y70
Y141
CP55940
(d) Detailed interaction of C−2 in site K
L125
F72
L126
T153
I129
T208
R149
Y132
L145
L133
(e) Detailed interaction of TBC in site K
Y207
I129
T208
H211
Y132
(f) Detailed interaction of CBD in site K
F200
G204
S203
Y207
I129
T208
Y132
H211
(g)
Residue Energy Contribution (kcal/mol)
ILE129
THR153
LEU144
LEU126
ARG149
LEU125
LEU145
LEU133
PHE72
Steric of C−2
Hbonding of C−2
Hydrophobic of C−2
(h)
ARG131
ARG302
TYR70
SER303
TYR141
SER69
TBC CBD
Residue Energy Contribution (kcal/mol)
Steric of CBD
Steric of TBC
Hbonding of CBD
Hbonding of TBC
Hydrophobic of CBD
Hydrophobic of TBC
(i)
ILE129
THR153
TYR132
LEU145
LEU126
LEU125
ARG149
PHE72
LEU133
THR208
TYR207
HIS211
PHE200
C−2 TBC CBD
Residue Energy Contribution (kcal/mol)
Steric of CBD
Steric of TBC
Steric of C−2
Hbonding of CBD
Hbonding of TBC
Hbonding of C−2
Hydrophobic of CBD
Hydrophobic of TBC
Hydrophobic of C−2

Figure 3 The detailed interactions and residue energy contribution of C-2, TBC and CBD in sites B, C and K. (a) The detailed binding pose of C-2 in site B. (b) The detailed binding pose of TBC in site C. (c) The detailed binding pose of CBD in site C. (d) The detailed binding pose of C-2 in site K. (e) The detailed binding pose of TBC in site K. (f) The detailed binding pose of CBD in site K. (g) The residue energy contribution of key residues for C-2 in site B. (h) The comparisons of residue energy contribution of key residues for TBC and CBD in site C. (i) The comparisons of residue energy contribution of key residues for C-2, TBC, and CBD in site K.

Site K is adjacent to site B. The distance between the centers of the two pockets is approximately 12 angstroms, of which the boundaries between them are about 3.6 angstroms. Site K was detected only by one algorithm; however, our predictions are supported by 3D structures of other GPCRs as mentioned previously, so we still considered site K when predicting potential allosteric binding sites. We docked C-2, TBC, and CBD into site K of CB2 to study their detailed interactions. As shown in Figure 2d–f, Y132$^{3.51}$ contributed hydrophobic and steric interactions to the binding of C-2 and TBC. Y207$^{5.56}$ forms strong hydrophobic and steric interactions with TBC as well as CBD. L126$^{3.45}$ contributes to steric interaction with C-2. In addition, I129$^{3.48}$ and T208$^{5.57}$ contributed to the steric and hydrophobic interactions among all three AMs. I129$^{3.48}$ is supported by crystal structures of ADRB2 and C5aR1 [98, 99]. In ADRB2, C125$^{3.44}$, V129$^{3.48,}$ and V210$^{5.49}$ create the binding site which is consistent with site K. Especially, at the position of 5.49, V210 has a high energy contribution to the binding of AS408. Meanwhile, W213$^{5.49}$ in C5aR1 also significantly contributes to the binding of NDT9513727 via its indole ring. Based on our docking results, we found that C-2 has a different binding pose with the highest docking scores, which are located in the TM3 and connected site B and site K. This explains why the residues T153$^{4.45}$ and I129$^{3.48}$ contribute most to the binding of C-2. T153$^{4.45}$ and I129$^{3.48}$ form strong steric interactions, meanwhile, I129$^{3.48}$ is also positioned to form a strong hydrophobic interaction with C-2 in site B.

Thus, this result further proves that T153$^{4.45}$ and I129$^{3.48}$ are highly possible key binding residues in TM 3,4, and 5[69].

3.3 Detailed Binding Poses and Interactions of AMs in Site G of CB2

As shown in Table 1, the docking energies of C-2, TBC, and CBD in site G were −6.34, −5.42, and −5.89 kcal/mol. As shown in Figure 3d, W158$^{4.50}$ was the critical residue that contributed greatly to the binding of AMs in site G. W158$^{4.50}$ was predicted to form a hydrogen bond with C-2, hydrophobic interactions with CBD, and strong steric interactions with all three AMs. Moreover, our results also showed that S75$^{2.45}$ formed a hydrogen bond with CBD and strong steric interaction with all AMs. In addition, L55$^{1.54}$ formed steric interaction with C-2 as well as CBD. L154$^{4.46}$ contributed to strong hydrophobic and steric interactions with C-2 in site G[69].

The key residues involved in the binding of C-2, TBC, and CBD were supported by the crystal structure of CB1-orthosteric CP55940-NAM ORG27569 as mentioned previously. For example, I245$^{4.54}$, T242$^{4.51}$, C238$^{4.47}$, V161$^{2.48}$, F237$^{4.46,}$ and W241$^{4.50}$ of CB1 contributed to the binding of ORG27569. Among those residues, W241$^{4.50}$ (CB1) and W158$^{4.50}$ (CB2) are highly conserved in class A GPCRs [66], and both are predicted to have a high energy contribution to the binding of AMs in CBs. Thus, we suggested that W158$^{4.50}$ and L154$^{4.46}$ may be the key binding residues in site G[69].

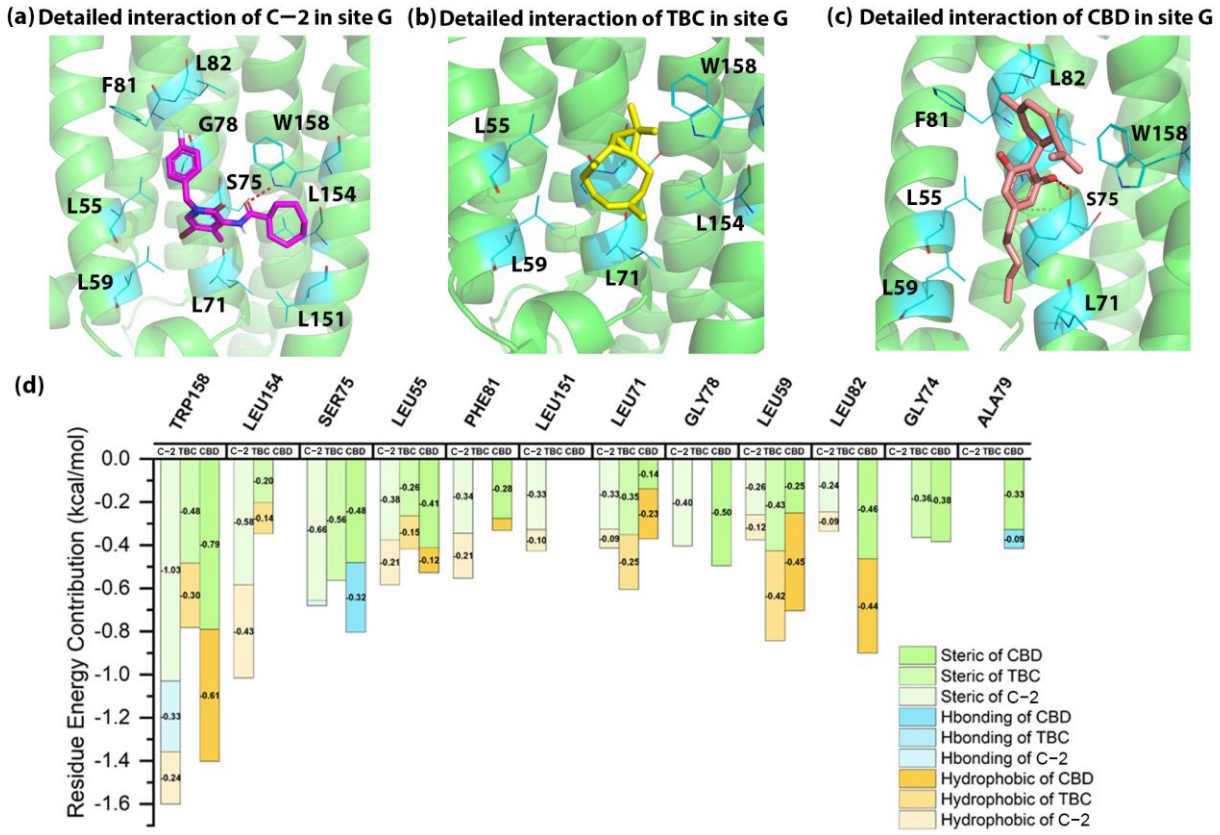

Figure 4. The detailed interactions and residue energy contribution of C-2, TBC and CBD in site G. (a) The detailed binding pose of C-2 in site G. (b) The detailed binding pose of TBC in site G. (c) The detailed binding pose of CBD in site G. (d) The comparisons of residue energy contribution of the key residues for these AMs in site G.

3.4 Detailed Binding Poses and Interactions of AMs in Site H of CB2

As shown in Table 1, the docking energies of C-2, TBC, and CBD in site H were −4.31, −2.79, and −4.21 kcal/mol respectively. The lower docking score for TBC was due to its smaller structure. When looking into the detailed interactions of C-2, TBC, and CBD in site H, there were steric and hydrophobic interactions along with only one hydrogen bonding. As shown in Figure 4,

H95$^{2.65}$ formed a weak hydrogen bond with C-2. K278$^{7.31}$ and K279$^{7.32}$ contributed the highest binding energy to the binding of C-2 in CB2. K278$^{7.31}$ formed steric and hydrophobic interactions with C-2, while K279$^{7.32}$ contributed to the steric interaction for the binding of all AMs and a hydrophobic interaction to that of TBC. F91$^{2.61}$ forms steric interaction with C-2 in site H. F281$^{7.34}$ also made contributions to the binding of C-2 via a hydrophobic interaction in site H[69].

Up to date, there is no available crystal or cryo-EM structure of receptor–AM to support this binding site. However, this allosteric site is supported by computational and biological validation, which is about the potential docking pose of D3R-selective antagonist R-22 in the crystal structure of human dopamine D3 receptor (D3R) [101]. For example, the authors suggested that the R-22 might extend to the binding site formed by TMs 1-2-7 region of D3R with eticlopride and have interactions with some key residues, such as E90$^{2.65}$. Based on the structure of eticlopride and R-22 in D3R, Lane, and co-workers [102] predicted another potential allosteric binding site that extends toward ECL2, formed by TM1, TM2, and TM7, which is at the same location of site H in Figure 1. The authors then conducted the virtual screening and identified some hit compounds as the AMs in their work. In addition, our previous work [103] also supported the binding site of site H, in which we docked the bitopic ligand-SB269652 into dopamine 2 receptor (D2R). Our docking results indicated that the allosteric fragment of SB269652 is bound to the allosteric binding site formed by TMs 1-2-7[69].

Although CB1 has the most similar sequence to CB2, it has not been demonstrated by X-ray crystal or cryo-EM structures that CB1 has an allosteric binding site in the same position as site H of CB2. Based on the structural alignment and our docking results, K278$^{7.31}$ and K279$^{7.32}$ of site H in CB2 refer to K376$^{7.31}$ and T377$^{7.32}$ in CB1, respectively. One of the key residues is the

histidine at the position of 2.65 at CB2 (H95) and CB1 (H178), which can form hydrogen bonds with ligands[69].

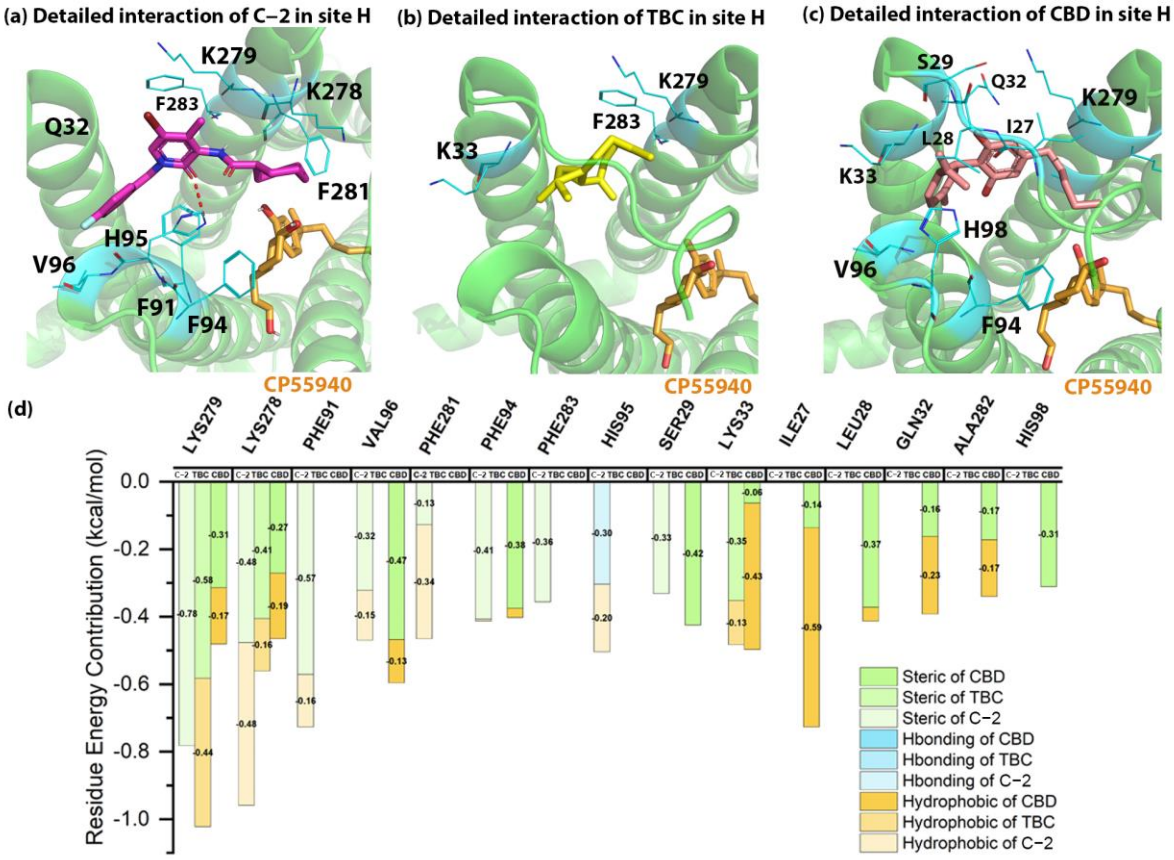

Figure 5. The detailed interactions and residue energy contribution of C-2, TBC and CBD in site H. (a) The detailed binding pose of C-2 in site H. (b) The detailed binding pose of TBC in site H. (c) The detailed binding pose of CBD in site H. (d) The comparisons of residue energy contribution of these AMs in site H.

3.5 Detailed Binding Poses and Interactions of AMs in Site I and J of CB2

The docking energies of C-2, TBC, and CBD in site I were −7.34, −6.39, and −5.92 kcal/mol, indicating the potential of site I in CB2. Comparing the detailed interactions of C-2 in site I, several strong steric and hydrophobic interactions were observed in the binding site. As illustrated in Figure 5, C-2 had a strong hydrophobic interaction with F202$^{5.51}$ and F259$^{6.49}$, forming strong steric interactions with F202$^{5.51}$ and A199$^{5.48}$. For TBC, it formed a steric interaction with F259$^{6.49}$ and a hydrophobic interaction with L262$^{6.52}$. In addition, CBD interacted with L255$^{6.45}$ via strong steric interaction and contacted F259$^{6.49}$ via a strong hydrophobic interaction (−1.4 kcal/mol). Since the residue energy contributions in site I was different among C-2, TBC and CBD, it was hard to say which residues were more important for the binding of AMs in CB2. But as for C-2, F202$^{5.51}$, A199$^{5.48,}$ and L262$^{6.52}$ were the potential key residues that contributed most to the binding with CB2 in site I[69].

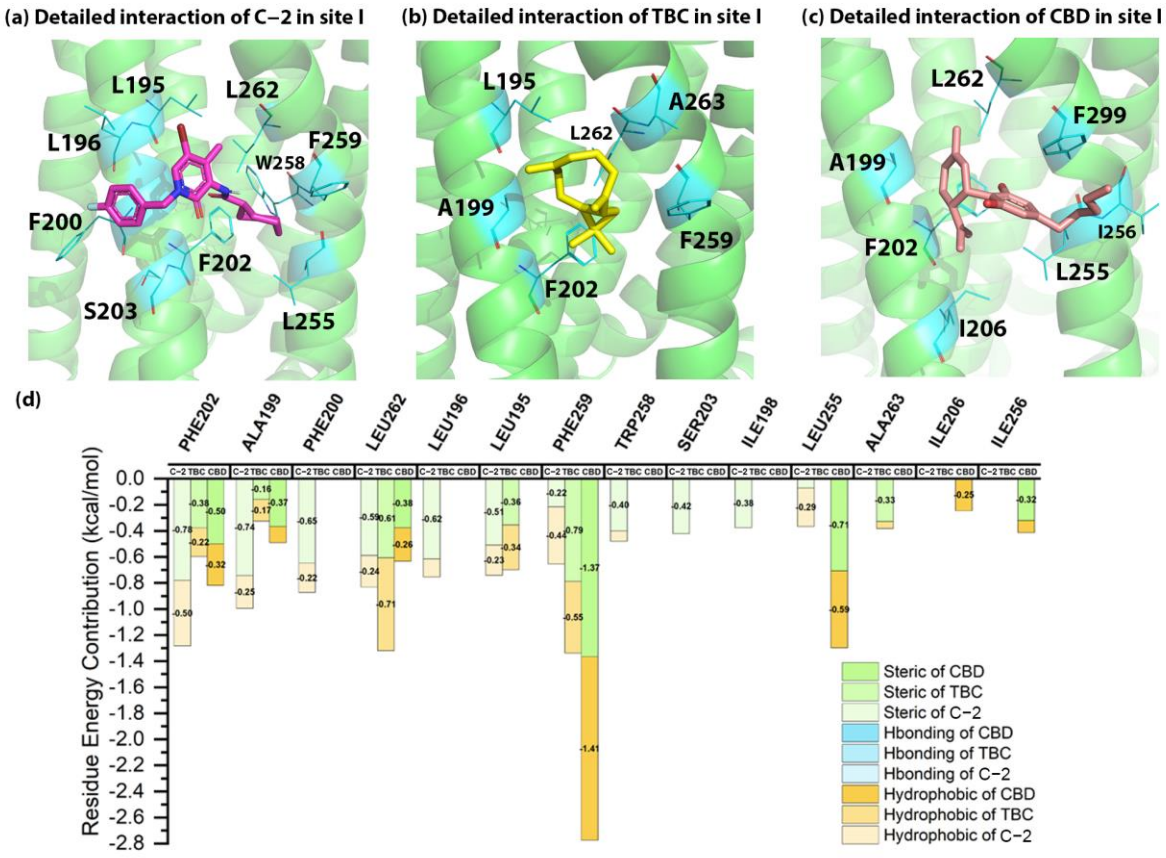

Figure 6. The detailed interactions and residue energy contribution of C-2, TBC and CBD in site I. (a) The detailed binding pose of C-2 in site I. (b) The detailed binding pose of TBC in site I. (c) The detailed binding pose of CBD in site I. (d) The comparisons of residue energy contribution of binding residues for these AMs in site I.

As illustrated in Table 1, the docking scores of three AMs in site J were not as good as those in sites B, G, and I. As shown in Figure 6, T25 contributed greatly to the binding of C-2, TBC, and CBD, including the hydrogen bonds with CBD and the hydrophobic/steric interactions with C-2 and TBC. In addition, E181 in site J also interacted with C-2 via a strong steric interaction, while L185 contacted CBD via steric and hydrophobic interactions. For site J, our docking results showed that T25 might be an important residue in this binding site[69].

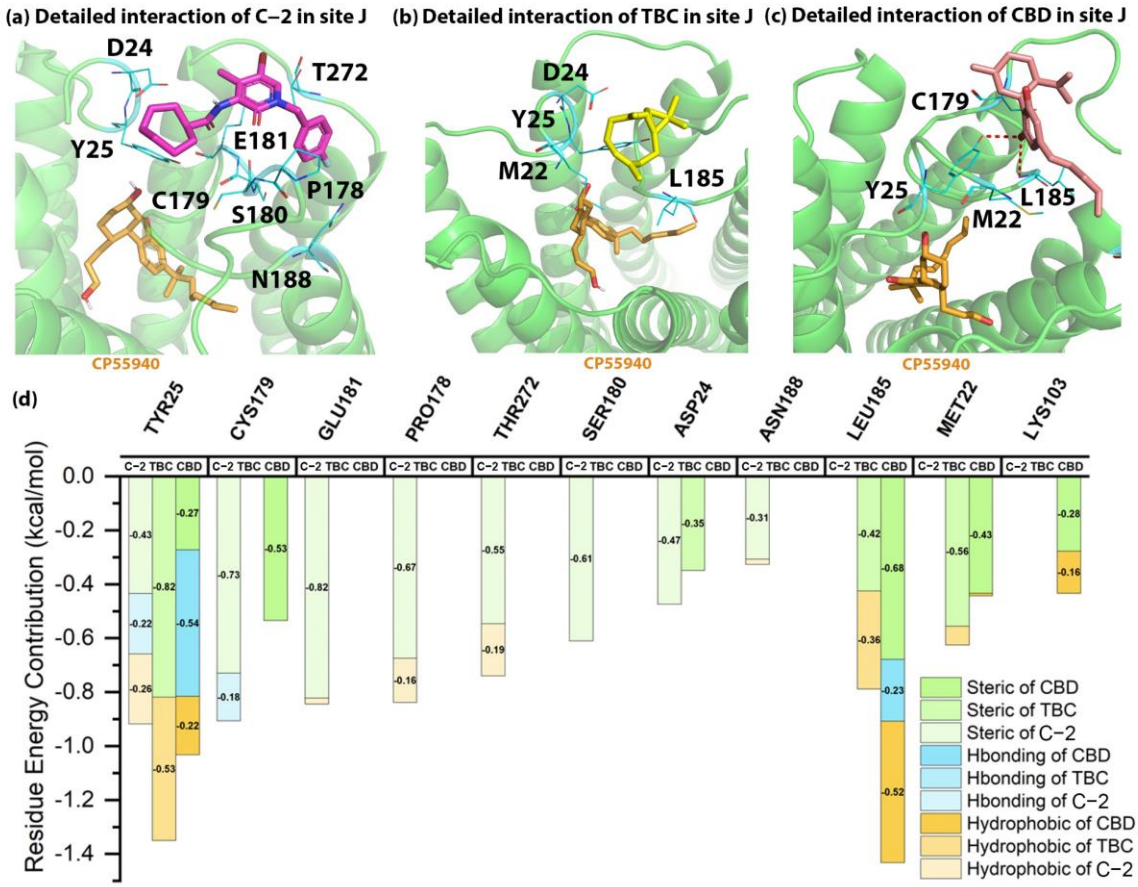

Figure 7. The detailed interactions and residue energy contribution of C-2, TBC and CBD in site J. (a) The detailed binding pose of C-2 in site J. (b) The detailed binding pose of TBC in site J. (c) The detailed binding pose of CBD in site J. (d) The comparisons of residue energy contribution of the binding residues for these AMs in site J.

3.6 MD Simulations for C-2 in Five Predicted Allosteric Binding Sites

Molecular dynamics (MD) simulations were performed for the five promising binding sites, namely, site B, site G, site H, site I, and site J. For each system, 250 snapshots were evenly

collected from the 150-ns MD trajectory after the system reached equilibrium for post-MD analysis. As shown in Figures 7 and 8, all the MD systems reached equilibrium after 20 ns. In Figure 8, only for site H and site I, the ligand can reside inside the binding pocket[69].

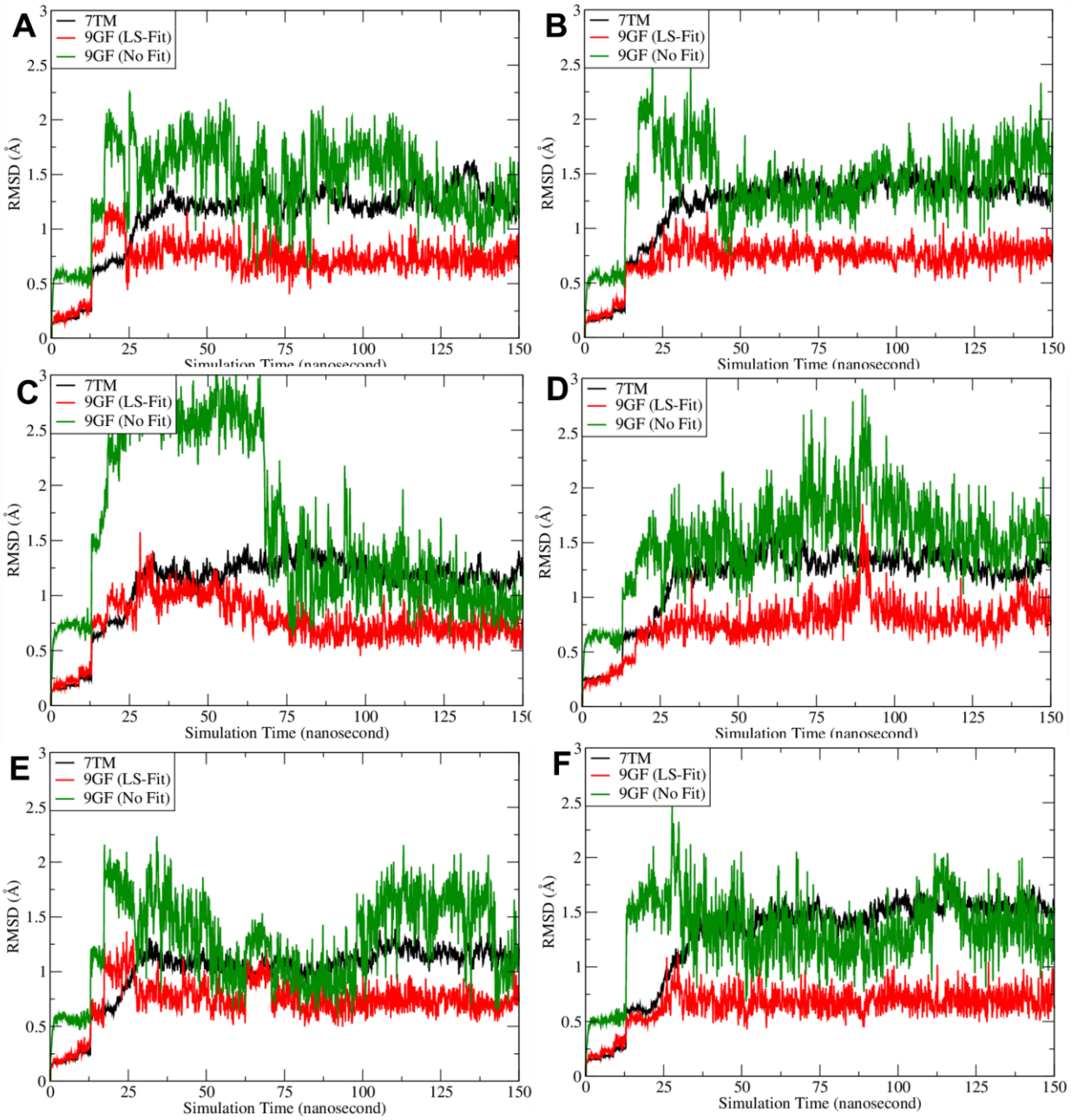

Figure 8. The time course of root–mean–square deviations (RMSD) of mainchain atoms of the transmembrane domains (7TM, black), heavy atoms of CP55940 after least-square (LS) fitting (9GF, red) and heavy atoms of CP55940 without fitting (9GF, green). To calculate the No-Fit RMSDs for CP55940, the

mainchain atoms of 7TM were first aligned and the resulting translation–rotation matrix were then applied to the ligand. After the coordinate transformation, the RMSDs were calculated directly. (A) CP55940/CB2 without C-2 binding, (B) site B, (C) site G, (D) site H, (E) site I and (F) site J.

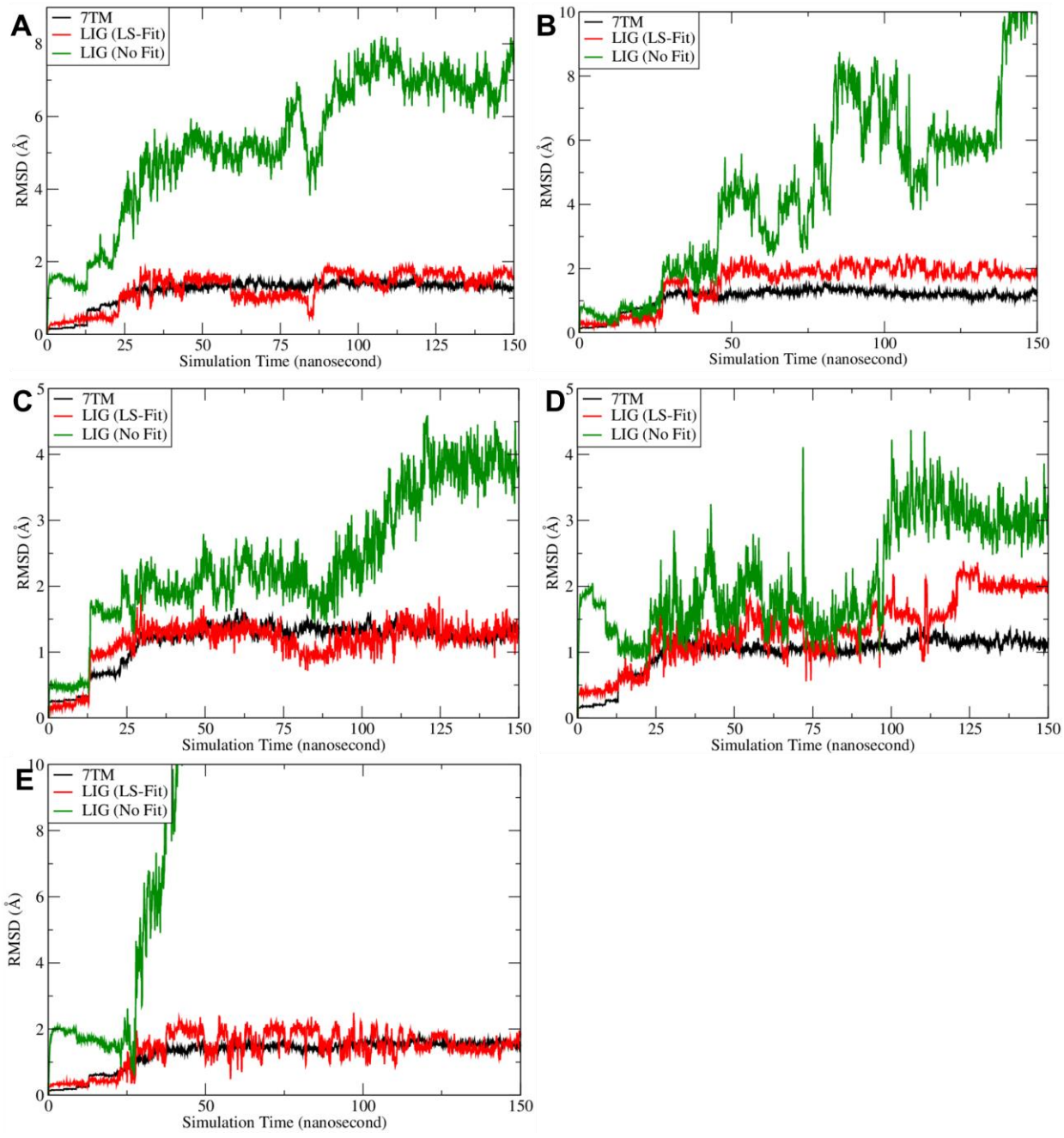

Figure 9. The time course of root–mean–square deviations of mainchain atoms of the transmembrane domains (7TM, black), heavy atoms of C-2 after least-square (LS) fitting (LIG, red) and heavy atoms of C-2

without fitting (LIG, green). To calculate the No-Fit RMSDs for C-2, the mainchain atoms of 7TM were first aligned and the resulting translation–rotation matrix were then applied to the ligand. After the coordinate transformation, the RMSDs were calculated directly. (A) site B, (B) site G, (C) site H, (D) site I and (E) site J.

The calculated molecular mechanics/Poisson-Boltzmann surface area-WSAS (MM-PBSA-WSAS) free energies for the CB2/CP55940/C-2 complex were summarized in Table 2. Site B has the best free energy of -6696.94 kcal/mol, which is significantly lower than other binding sites. We further calculated the binding free energies between CB2 and C-2 (Table 3) as well as CB2 and CP55940 (Table 4). As shown in Table 3, the binding between CB2 and C-2 are weak for all the sites except for site H, for which the calculated MM-PBSA-WSAS binding free energy is -15.18 kcal/mol. When we consider CP55940 as a part of the receptor, the binding between CB2 and C-2 is even stronger with the binding free energy, -19.20 kcal/mol. However, in site B and site J, C-2 bound to CB2 results in positive binding free energy, indicating that these two sites are less likely to be the allosteric binding sites. Interestingly, the binding between CP55940 and CB2 is weakened for most binding sites, except for site H* as shown in Table 4. The MM-PBSA-WSAS binding free energy, -35.25 kcal/mol when C-2 is absent from the complex, can be considered as the reference to predict if C-2 is a PAM or NAM. Taking all three analyses of binding free energy into consideration, we mainly focused on-site H. With C-2 residing at site H, the MM-PBSA-WSAS of CP55940 binding, -32.98 kcal/mol, is slightly worse than the control suggesting C-2 is a NAM. However, site H is adjacent to the orthosteric site and C-2 and CP55940 have a favorable interaction between them. Thus, C-2 should be considered as a part of the receptor when calculating the binding free energy of CP55940. With C-2 being considered as a part of the receptor (labeled as H* in Table 4), the calculated MM-PBSA-WSAS binding free energy is -37.01

kcal/mol, about 2.27 kcal/mol more potent than the control. Thus, C-2 is a PAM under this circumstance. Considering the MM-PBSA-WSAS free energies of the complexes have large fluctuation, the predicted absolute free energies of complexes may not be very reliable. Based on the MD trajectory stability (RMSD ~ Simulation time plots) and binding free energy results, siteH is the most possible binding site the ligand resides in[69].

Table 2. Energy decomposition of MM-PBSA-WSAS free energy for the CB2/CP55940/C-2 complex. All energies are in kcal/mol.

Site	E_{VDW}	E_{eel}	E_{int}	G_{pol}	G_{nonpol}	TS	$G_{MM-PBSA}$
B	-1258.20 ± 1.76	-6285.24 ± 5.71	7136.34 ± 25.51	-2967.96 ± 16.65	87.88 ± 0.13	3409.76 ± 0.72	-6696.94 ± 16.46
G	-1265.15 ± 2.80	-6381.82 ± 6.19	7129.29 ± 24.64	-2569.41 ± 4.20	88.41 ± 0.06	3406.67 ± 0.36	-6405.35 ± 21.17
H	-1200.43 ± 2.23	-6312.41 ± 4.79	7132.86 ± 23.21	-2866.26 ± 4.28	92.67 ± 0.12	3420.62 ± 0.46	-6574.19 ± 25.13
I	-1262.70 ± 3.64	-6329.59 ± 8.27	7131.64 ± 21.23	-2837.03 ± 2.29	87.48 ± 0.06	3404.49 ± 0.58	-6614.69 ± 14.00
J	-1189.50 ± 5.66	-6281.94 ± 9.95	7121.55 ± 20.61	-2904.44 ± 25.48	95.04 ± 0.17	3425.12 ± 0.76	-6584.40 ± 11.26

E_{VDW}: Van der Waals energy; E_{eel}: Electrostatic energy; E_{int}: Internal energy; G_{pol}: the polar part of solvation free energy; G_{nonpol}: the nonpolar part of solvation free energy; TS: the entropy contribution of the MM-PBSA free energy; $G_{MM-PBSA}$: MM-PBSA free energy.

Table 3. Energy decomposition of MM-PBSA-WSAS free energy for C-2 binding to CB2 with CP55940 residing in the orthosteric site. All energies are in kcal/mol.

Site	ΔE_{VDW}	ΔE_{eel}	ΔG_{pol}	ΔG_{nonpo}	$T\Delta S$	$\Delta G_{MM\text{-}PBSA}$
B	-27.18 ± 0.27	-9.38 ± 0.20	21.57 ± 0.19	-2.56 ± 0.0S2	-18.10 ± 0.12	0.55 ± 0.22
G	-26.71 ± 0.53	-3.80 ± 0.24	10.15 ± 0.29	-2.00 ± 0.04	-16.69 ± 0.05	-5.66 ± 0.16
H	-52.41 ± 0.61	-9.01 ± 0.58	25.64 ± 0.42	-4.25 ± 0.01	-24.85 ± 0.13	-15.18 ± 0.58
H*	-55.71 ± 0.61	-8.83 ± 0.57	23.66 ± 0.44	-4.25 ± 0.01	-25.92 ± 0.11	-19.20 ± 0.57
I	-30.03 ± 0.25	-4.90 ± 0.10	10.56 ± 0.05	-2.51 ± 0.04	-18.34 ± 0.11	-8.55 ± 0.15
J	-32.52 ± 0.84	-0.35 ± 0.38	22.64 ± 0.86	-2.78 ± 0.04	-19.22 ± 0.29	6.20 ± 0.81

H* implies that the C-2 is considered as a part of the receptor. E_{VDW}: Van der Waals energy; E_{eel}: Electrostatic energy; G_{pol}: the polar part of solvation free energy; G_{nonpol}: the nonpolar part of solvation free energy; $T\Delta S$： the entropy contribution for ligand binding at temperature T; $G_{MM\text{-}PBSA}$: MM-PBSA free energy.

Table 4. Energy decomposition of MM-PBSA-WSAS free energy for CP55940 binding to CB2 with C-2, an allosteric agonist existing. All energies are in kcal/mol.

Site	ΔE_{VDW}	ΔE_{eel}	ΔG_{pol}	ΔG_{nonpo}	$T\Delta S$	$\Delta G_{MM\text{-}PBSA}$
No Ligand	-57.62 ± 0.13	-25.25 ± 0.33	26.14 ± 0.32	-4.81 ± 0.01	-26.29 ± 0.03	-35.25 ± 0.28
B	-58.03 ± 0.06	-20.01 ± 0.28	25.45 ± 0.12	-4.94 ± 0.01	-25.88 ± 0.05	-31.65 ± 0.21
G	-57.50 ± 0.27	-24.93 ± 0.72	26.79 ± 0.26	-4.80 ± 0.01	-26.44 ± 0.07	-33.99 ± 0.28
H	-51.53 ± 0.17	-28.43 ± 0.15	26.74 ± 0.15	-4.86 ± 0.01	-25.09 ± 0.06	-32.98 ± 0.14
H*	-54.82 ± 0.17	-28.25 ± 0.15	24.76 ± 0.12	-4.86 ± 0.01	-26.16 ± 0.03	-37.01 ± 0.13
I	-56.27 ± 0.27	-22.77 ± 0.29	25.97 ± 0.12	-4.92 ± 0.01	-25.56 ± 0.07	-32.43 ± 0.34

J	-57.75 ± 0.23	-21.95 ± 0.18	25.78 ± 0.07	-4.86 ± 0.01	-26.11 ± 0.05	-32.67 ± 0.09

H* implies that the C-2 is considered as a part of the receptor. E_{VDW}: Van der Waals energy; E_{eel}: Electrostatic energy; G_{pol}: the polar part of solvation free energy; G_{nonpol}: the nonpolar part of solvation free energy; $T\Delta S$： the entropy contribution for ligand binding at temperature T; $G_{MM\text{-}PBSA}$: MM-PBSA free energy.

The C-2 binding mode before and after MD simulations is illustrated by Figure 9A, C. Note that the crystal structure and the representative MD conformation were aligned so that one can compare them directly. We found that CP55940 has insignificant changes before and after MD simulations (Figures 7D and 9A, C), while C-2 undergoes significant changes (Figures 8C and 9A, C). The surrounding residues shown in Figure 9B are for the crystal structure and docking conformation, whereas those in Figure 9D are for the representative MD conformation. Note that CP55940 forms two hydrogen bonds with $S285^{7.38}$ and L182, and C-2 forms two hydrogen bonds with $H95^{2.65}$ and $K278^{7.31}$. Those residues could be candidates for the mutagenesis experiment to confirm the proposed binding mechanism, i.e., C-2 binds at site H and it can boost the activity of CP55940 binding to CB2[69].

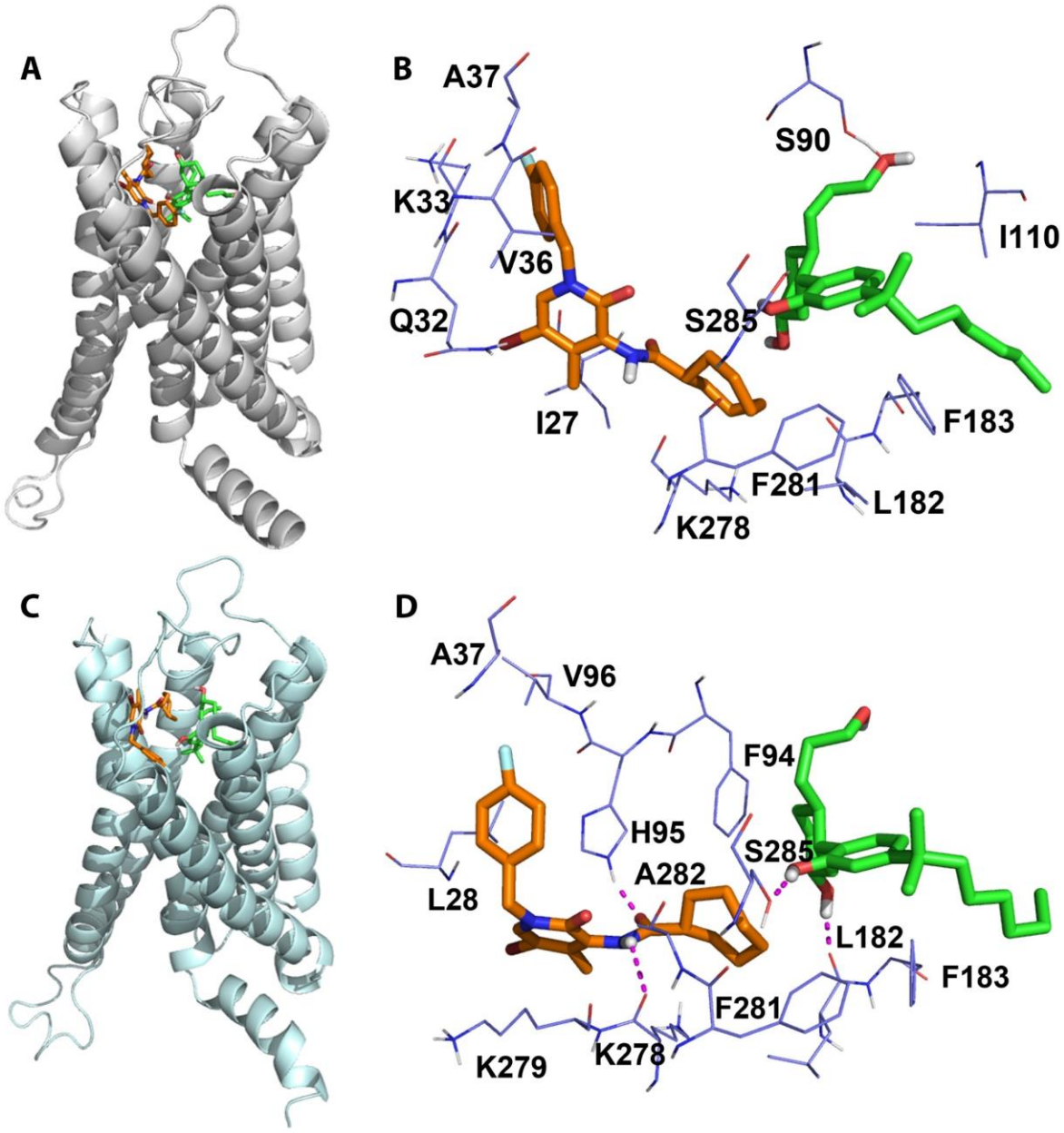

Figure 10. The detailed interactions between C-2, CP55940, and CB2 receptor where C-2 resides in site H. (A) The crystal structure of CP55940/CB2 with C-2, the PAM binding at site H. (B) The CB2 residues surrounding CP55940 and C-2. (C) The representative MD structure (the one that is structurally most similar to the average structure). (D) The residues surrounding CP55940 and C-2 in the representative MD structure. Two hydrogen bonds are formed between C-2 and CB2 residues (H95$^{2.65}$, and K278$^{7.31}$), and two hydrogen bond is formed between CP55940 and CB2 residues (S285$^{7.38}$ and L182). The hydrogen bonds are shown as magenta dashed lines.

4.0 Conclusions

In our previous research, we found that the binding of allosteric modulators did not cause a significant impact on the conformational change for both orthosteric and allosteric binding sites of a target protein. In the present work, among seven predicted binding sites, sites B, K, G, and C are supported by the known crystal structures of other class A GPCRs [66, 92, 93, 95-97, 99, 104]. While site H has a supporting of computational and biological validation [102]. For example, we found that both site K and site B are supported by crystal structures of ADRB2 coupled with orthosteric antagonists or agonist, respectively. Site K is shown to bind with NAMs of C5aR1 human receptor and ADRB2 human receptor while site B has been supported by the ADRB2 human receptor which binds with a PAM. The crystal structure of FFaR1 human receptor–PAM complex [93] gives us another supporting that after aligning CB2 and FFaR1 human receptor, the position of PAM is inserted into site B, but the tail of the PAM is connected to site K. Thus, site B is more likely to bind with PAMs, while sites C, G, and K have higher possibility to bind with NAMs. However, based on the results of MD simulations, site H is the most possible binding site of CB2 for the allosteric binding of C-2. It may be because site H is adjacent to the orthosteric site and C-2 can directly have a favorable interaction with CP55940. We then selected some potential key binding residues, for example, T153$^{4.45}$, I129$^{3.48}$, and R149$^{4.41}$ in site B, and K278$^{7.31}$ and K279$^{7.32}$ in site H, which will undergo further bio-validation. Among the residues of site H, H95$^{2.65}$ and S285$^{7.38}$ may be the important binding residues that form hydrogen bonds with C-2. The H95$^{2.65}$ and S285$^{7.38}$ in CB2 refer to H178$^{2.65}$ and S383$^{7.38}$ in CB1, respectively. Thinking about the selectivity in receptor subtypes, if these residues are key binding residues, CB1 may form the same interactions (hydrogen bonds) as CB2, which is not ideal for designing an AM that selectively

targets on CB2. Ligand selectivity is always a challenging problem for researchers to understand or to deal with, not only for orthosteric ligands but also for AMs [105]. So much more effort should be taken to study, compare and analyze the high-resolution structures of CB1 and CB2. Taking the supporting crystal structures (e.g., ADRB2 human receptor) into consideration, the allosteric modulators with different properties may have different binding sites. The potential key residues in each site, especially for those supported by the crystal structures, provide a new sight for designing unique AMs for specific binding sites[69]. In the future, we would like to perform site-direct mutagenesis to further validate our selected potential key binding residues in both site B and site H. We will also conduct fragment-based drug design as well as scaffold hopping to discover novel categories of CB2 AMs.

Bibliography

1. Di Marzo, V., *New approaches and challenges to targeting the endocannabinoid system.* Nat Rev Drug Discov, 2018. **17**(9): p. 623-639.
2. Manzanares, J., et al., *Role of the endocannabinoid system in drug addiction.* Biochem Pharmacol, 2018. **157**: p. 108-121.
3. Basavarajappa, B.S., et al., *Endocannabinoid system in neurodegenerative disorders.* J Neurochem, 2017. **142**(5): p. 624-648.
4. Garani, R., J.J. Watts, and R. Mizrahi, *Endocannabinoid system in psychotic and mood disorders, a review of human studies.* Prog Neuropsychopharmacol Biol Psychiatry, 2021. **106**: p. 110096.
5. Fowler, C.J., *The endocannabinoid system - current implications for drug development.* J Intern Med, 2021. **290**(1): p. 2-26.
6. Jung, K.M., L. Lin, and D. Piomelli, *The endocannabinoid system in the adipose organ.* Rev Endocr Metab Disord, 2021.
7. Jansma, J., et al., *Targeting the endocannabinoid system with microbial interventions to improve gut integrity.* Prog Neuropsychopharmacol Biol Psychiatry, 2021. **106**: p. 110169.
8. Spanagel, R., *Cannabinoids and the endocannabinoid system in reward processing and addiction: from mechanisms to interventions*[P SEP]Dialogues Clin Neurosci, 2020. **22**(3): p. 241-250.
9. Morales, P. and N. Jagerovic, *Novel approaches and current challenges with targeting the endocannabinoid system.* Expert Opinion on Drug Discovery, 2020. **15**(8): p. 917-930.
10. Leyva-Illades, D. and S. Demorrow, *Orphan G protein receptor GPR55 as an emerging target in cancer therapy and management.* Cancer Manag Res, 2013. **5**: p. 147-55.
11. Reyes-Resina, I., et al., *Molecular and functional interaction between GPR18 and cannabinoid CB(2) G-protein-coupled receptors. Relevance in neurodegenerative diseases.* Biochem Pharmacol, 2018. **157**: p. 169-179.
12. Cao, J.K., J. Kaplan, and N. Stella, *ABHD6: Its Place in Endocannabinoid Signaling and Beyond.* Trends Pharmacol Sci, 2019. **40**(4): p. 267-277.
13. Brunetti, L., et al., *New Approaches to Cancer Therapy: Combining Fatty Acid Amide Hydrolase (FAAH) Inhibition with Peroxisome Proliferator-Activated Receptors (PPARs) Activation.* J Med Chem, 2019. **62**(24): p. 10995-11003.
14. Scherma, M., et al., *Interactions between the endocannabinoid and nicotinic cholinergic systems: preclinical evidence and therapeutic perspectives.* Psychopharmacology (Berl), 2016. **233**(10): p. 1765-77.
15. Sadanandan, S.M., et al., *Cannabinoid type 2 receptors inhibit GABAA receptor-mediated currents in cerebellar Purkinje cells of juvenile mice.* PLoS One, 2020. **15**(5): p. e0233020.
16. Herkenham, M., et al., *Characterization and localization of cannabinoid receptors in rat brain: a quantitative in vitro autoradiographic study.* J Neurosci, 1991. **11**(2): p. 563-83.
17. Chanda, D., D. Neumann, and J.F.C. Glatz, *The endocannabinoid system: Overview of an emerging multi-faceted therapeutic target.* Prostaglandins Leukot Essent Fatty Acids, 2019. **140**: p. 51-56.

18. Navarro, G., et al., *Targeting Cannabinoid CB2 Receptors in the Central Nervous System. Medicinal Chemistry Approaches with Focus on Neurodegenerative Disorders.* Front Neurosci, 2016. **10**: p. 406.
19. Munro, S., K.L. Thomas, and M. Abu-Shaar, *Molecular characterization of a peripheral receptor for cannabinoids.* Nature, 1993. **365**(6441): p. 61-5.
20. Cassano, T., et al., *Cannabinoid Receptor 2 Signaling in Neurodegenerative Disorders: From Pathogenesis to a Promising Therapeutic Target.* Front Neurosci, 2017. **11**: p. 30.
21. Fonseca, B.M., N.A. Teixeira, and G. Correia-da-Silva, *Cannabinoids as Modulators of Cell Death: Clinical Applications and Future Directions.* Rev Physiol Biochem Pharmacol, 2017. **173**: p. 63-88.
22. Gado, F., et al., *Allosteric modulators targeting cannabinoid cb1 and cb2 receptors: implications for drug discovery.* Future Med Chem, 2019. **11**(15): p. 2019-2037.
23. Chen, D.-j., et al., *Brain cannabinoid receptor 2: expression, function and modulation.* Acta Pharmacologica Sinica, 2017. **38**(3): p. 312-316.
24. Saldaña-Shumaker, S.L., A.J. Grenning, and C.W. Cunningham, *Modern approaches to the development of synthetic cannabinoid receptor probes.* Pharmacol Biochem Behav, 2021. **203**: p. 173119.
25. Xing, C., et al., *Cryo-EM Structure of the Human Cannabinoid Receptor CB2-G(i) Signaling Complex.* Cell, 2020. **180**(4): p. 645-654.e13.
26. Li, X., et al., *Crystal Structure of the Human Cannabinoid Receptor CB2.* Cell, 2019. **176**(3): p. 459-467.e13.
27. Shao, Z., et al., *High-resolution crystal structure of the human CB1 cannabinoid receptor.* Nature, 2016. **540**(7634): p. 602-606.
28. Hua, T., et al., *Activation and Signaling Mechanism Revealed by Cannabinoid Receptor-Gi Complex Structures.* Cell, 2020. **180**(4): p. 655-665.e18.
29. Kind, L. and P. Kursula, *Structural properties and role of the endocannabinoid lipases ABHD6 and ABHD12 in lipid signalling and disease.* Amino Acids, 2019. **51**(2): p. 151-174.
30. Gado, F., et al., *Identification of the First Synthetic Allosteric Modulator of the CB2 Receptors and Evidence of Its Efficacy for Neuropathic Pain Relief.* J Med Chem, 2019. **62**(1): p. 276-287.
31. Garai, S., et al., *B-973, a Novel α7 nAChR Ago-PAM: Racemic and Asymmetric Synthesis, Electrophysiological Studies, and in Vivo Evaluation.* ACS Med Chem Lett, 2018. **9**(11): p. 1144-1148.
32. Garai, S., et al., *Design, synthesis, and pharmacological profiling of cannabinoid 1 receptor allosteric modulators: Preclinical efficacy of C2-group GAT211 congeners for reducing intraocular pressure.* Bioorg Med Chem, 2021. **50**: p. 116421.
33. Wold, E.A., et al., *Allosteric Modulation of Class A GPCRs: Targets, Agents, and Emerging Concepts.* J Med Chem, 2019. **62**(1): p. 88-127.
34. Gaoni, Y. and R. Mechoulam, *Isolation, structure, and partial synthesis of an active constituent of hashish.* Journal of the American chemical society, 1964. **86**(8): p. 1646-1647.
35. Stasiulewicz, A., et al., *A Guide to Targeting the Endocannabinoid System in Drug Design.* Int J Mol Sci, 2020. **21**(8).
36. Sam, A.H., V. Salem, and M.A. Ghatei, *Rimonabant: From RIO to Ban.* J Obes, 2011. **2011**: p. 432607.

37. Kooistra, A.J., et al., *GPCRdb in 2021: integrating GPCR sequence, structure and function.* Nucleic Acids Research, 2021. **49**(D1): p. D335-D343.
38. Pándy-Szekeres, G., et al., *The G protein database, GproteinDb.* Nucleic Acids Research, 2022. **50**(D1): p. D518-D525.
39. Hauser, A.S., et al., *Trends in GPCR drug discovery: new agents, targets and indications.* Nature Reviews Drug Discovery, 2017. **16**(12): p. 829-842.
40. Wu, Y., et al., *GPCR Allosteric Modulator Discovery.* Adv Exp Med Biol, 2019. **1163**: p. 225-251.
41. Jacobson, K.A. and J.-M. Boeynaems, *P2Y nucleotide receptors: promise of therapeutic applications.* Drug Discovery Today, 2010. **15**(13): p. 570-578.
42. Wood, A. and D. Armour, *The discovery of the CCR5 receptor antagonist, UK-427,857, a new agent for the treatment of HIV infection and AIDS.* Prog Med Chem, 2005. **43**: p. 239-71.
43. Müller, C.E., A.C. Schiedel, and Y. Baqi, *Allosteric modulators of rhodopsin-like G protein-coupled receptors: Opportunities in drug development.* Pharmacology & Therapeutics, 2012. **135**(3): p. 292-315.
44. Flores-Otero, J., et al., *Ligand-specific endocytic dwell times control functional selectivity of the cannabinoid receptor 1.* Nat Commun, 2014. **5**: p. 4589.
45. Ibsen, M.S., M. Connor, and M. Glass, *Cannabinoid CB(1) and CB(2) Receptor Signaling and Bias.* Cannabis Cannabinoid Res, 2017. **2**(1): p. 48-60.
46. Luttrell, L.M. and D. Gesty-Palmer, *Beyond desensitization: physiological relevance of arrestin-dependent signaling.* Pharmacol Rev, 2010. **62**(2): p. 305-30.
47. Turu, G. and L. Hunyady, *Signal transduction of the CB1 cannabinoid receptor.* J Mol Endocrinol, 2010. **44**(2): p. 75-85.
48. Al-Zoubi, R., P. Morales, and P.H. Reggio, *Structural Insights into CB1 Receptor Biased Signaling.* Int J Mol Sci, 2019. **20**(8).
49. Ferrisi, R., et al., *Medicinal Chemistry approach, pharmacology and neuroprotective benefits of CB(2)R modulators in neurodegenerative diseases.* Pharmacol Res, 2021. **170**: p. 105607.
50. Liu, Q.R., et al., *Species differences in cannabinoid receptor 2 (CNR2 gene): identification of novel human and rodent CB2 isoforms, differential tissue expression and regulation by cannabinoid receptor ligands.* Genes Brain Behav, 2009. **8**(5): p. 519-30.
51. Demuth, D.G. and A. Molleman, *Cannabinoid signalling.* Life Sci, 2006. **78**(6): p. 549-63.
52. Zoratti, C., et al., *Anandamide initiates Ca(2+) signaling via CB2 receptor linked to phospholipase C in calf pulmonary endothelial cells.* Br J Pharmacol, 2003. **140**(8): p. 1351-62.
53. Alqarni, M., et al., *Examining the critical roles of human CB2 receptor residues Valine 3.32 (113) and Leucine 5.41 (192) in ligand recognition and downstream signaling activities.* Biochem Biophys Res Commun, 2014. **452**(3): p. 334-9.
54. Ranieri, R., et al., *Phytocannabinoids and Cannabimimetic Drugs: Recent Patents in Central Nervous System Disorders.* Recent Pat CNS Drug Discov, 2016. **10**(2): p. 157-177.
55. Schonhofen, P., et al., *Cannabinoid-Based Therapies and Brain Development: Potential Harmful Effect of Early Modulation of the Endocannabinoid System.* CNS Drugs, 2018. **32**(8): p. 697-712.
56. Dos Santos, R.G., J.E.C. Hallak, and J.A.S. Crippa, *Neuropharmacological Effects of the Main Phytocannabinoids: A Narrative Review.* Adv Exp Med Biol, 2021. **1264**: p. 29-45.

57. Zou, S. and U. Kumar, *Cannabinoid Receptors and the Endocannabinoid System: Signaling and Function in the Central Nervous System.* Int J Mol Sci, 2018. **19**(3).
58. Pacher, P., S. Bátkai, and G. Kunos, *The endocannabinoid system as an emerging target of pharmacotherapy.* Pharmacol Rev, 2006. **58**(3): p. 389-462.
59. Soethoudt, M., et al., *Cannabinoid CB(2) receptor ligand profiling reveals biased signalling and off-target activity.* Nat Commun, 2017. **8**: p. 13958.
60. Yang, D., et al., *G protein-coupled receptors: structure- and function-based drug discovery.* Signal Transduct Target Ther, 2021. **6**(1): p. 7.
61. Zhang, X., S. Dong, and F. Xu, *Structural and Druggability Landscape of Frizzled G Protein-Coupled Receptors.* Trends Biochem Sci, 2018. **43**(12): p. 1033-1046.
62. Vásquez, C. and D.L. Lewis, *The CB1 Cannabinoid Receptor Can Sequester G-Proteins, Making Them Unavailable to Couple to Other Receptors.* The Journal of Neuroscience, 1999. **19**(21): p. 9271.
63. Smith, J.S., R.J. Lefkowitz, and S. Rajagopal, *Biased signalling: from simple switches to allosteric microprocessors.* Nature Reviews Drug Discovery, 2018. **17**(4): p. 243-260.
64. Wootten, D., et al., *Mechanisms of signalling and biased agonism in G protein-coupled receptors.* Nature Reviews Molecular Cell Biology, 2018. **19**(10): p. 638-653.
65. Feng, Z., et al., *Binding Characterization of GPCRs-Modulator by Molecular Complex Characterizing System (MCCS).* ACS Chem Neurosci, 2020. **11**(20): p. 3333-3345.
66. Shao, Z., et al., *Structure of an allosteric modulator bound to the CB1 cannabinoid receptor.* Nat Chem Biol, 2019. **15**(12): p. 1199-1205.
67. Petrucci, V., et al., *Pepcan-12 (RVD-hemopressin) is a CB2 receptor positive allosteric modulator constitutively secreted by adrenals and in liver upon tissue damage.* Scientific Reports, 2017. **7**(1).
68. Navarro, G., et al., *Design of Negative and Positive Allosteric Modulators of the Cannabinoid CB2 Receptor Derived from the Natural Product Cannabidiol.* Journal of Medicinal Chemistry, 2021. **64**(13): p. 9354-9364.
69. Yuan, J., et al., *In Silico Prediction and Validation of CB2 Allosteric Binding Sites to Aid the Design of Allosteric Modulators.* Molecules, 2022. **27**(2).
70. Feng, Z., et al., *Modeling, molecular dynamics simulation, and mutation validation for structure of cannabinoid receptor 2 based on known crystal structures of GPCRs.* J Chem Inf Model, 2014. **54**(9): p. 2483-99.
71. Berman, H.M., et al., *The Protein Data Bank.* Nucleic Acids Res, 2000. **28**(1): p. 235-42.
72. Goodsell, D.S., et al., *RCSB Protein Data Bank: Enabling biomedical research and drug discovery.* Protein Sci, 2020. **29**(1): p. 52-65.
73. Sain, N.M.H., et al., *Antinociceptive effects of the non-selective cannabinoid receptor agonist CP 55,940 are absent in CB1−/− and not CB2−/− mice in models of acute and persistent pain.* Neuropharmacology, 2009. **57**(3): p. 235-241.
74. Panjkovich, A. and X. Daura, *PARS: a web server for the prediction of protein allosteric and regulatory sites.* Bioinformatics, 2014. **30**(9): p. 1314-1315.
75. Chen, M., et al., *MCCS, a novel characterization method for protein-ligand complex.* Brief Bioinform, 2021. **22**(4).
76. Pettersen, E.F., et al., *UCSF Chimera--a visualization system for exploratory research and analysis.* J Comput Chem, 2004. **25**(13): p. 1605-12.

77. Shapovalov, M.V. and R.L. Dunbrack, Jr., *A smoothed backbone-dependent rotamer library for proteins derived from adaptive kernel density estimates and regressions.* Structure, 2011. **19**(6): p. 844-58.
78. Pedretti, A., L. Villa, and G. Vistoli, *VEGA – An open platform to develop chemo-bio-informatics applications, using plug-in architecture and script programming.* Journal of Computer-Aided Molecular Design, 2004. **18**(3): p. 167-173.
79. Olsson, M.H.M., et al., *PROPKA3: Consistent Treatment of Internal and Surface Residues in Empirical pKa Predictions.* Journal of Chemical Theory and Computation, 2011. **7**(2): p. 525-537.
80. Søndergaard, C.R., et al., *Improved Treatment of Ligands and Coupling Effects in Empirical Calculation and Rationalization of pKa Values.* Journal of Chemical Theory and Computation, 2011. **7**(7): p. 2284-2295.
81. Li, H., K. Leung, and M.-H. Wong, *Idock: A multithreaded virtual screening tool for flexible ligand docking.* 2012 IEEE Symposium on Computational Intelligence in Bioinformatics and Computational Biology (CIBCB), 2012.
82. Morris, G.M., et al., *AutoDock4 and AutoDockTools4: Automated docking with selective receptor flexibility*. Journal of computational chemistry, 2009. **30**(16): p. 2785-2791.
83. Trott, O. and A.J. Olson, *AutoDock Vina: improving the speed and accuracy of docking with a new scoring function, efficient optimization, and multithreading.* J Comput Chem, 2010. **31**(2): p. 455-61.
84. Jorgensen, W.L., et al., *Comparison of simple potential functions for simulating liquid water*. The Journal of Chemical Physics, 1983. **79**(2): p. 926-935.
85. Maier, J.A., et al., *ff14SB: Improving the Accuracy of Protein Side Chain and Backbone Parameters from ff99SB.* J Chem Theory Comput, 2015. **11**(8): p. 3696-713.
86. Hou, T., et al., *Assessing the performance of the MM/PBSA and MM/GBSA methods. 1. The accuracy of binding free energy calculations based on molecular dynamics simulations.* J. Chem. Inf. Model., 2011. **51**(1): p. 69-82.
87. Hou, T., et al., *Assessing the performance of the molecular mechanics/Poisson Boltzmann surface area and molecular mechanics/generalized Born surface area methods. II. The accuracy of ranking poses generated from docking.* J. Comput. Chem., 2011. **32**(5): p. 866-77.
88. Case, D.A., et al., *AMBER 2018.* University of California, San Francisco. https://ambermd.org/, 2018.
89. Wray, R., et al., *Novel MscL agonists that allow multiple antibiotics cytoplasmic access activate the channel through a common binding site.* PLOS ONE, 2020. **15**(1): p. e0228153.
90. Wang, J. and T. Hou, *Develop and Test a Solvent Accessible Surface Area-Based Model in Conformational Entropy Calculations.* Journal of Chemical Information and Modeling, 2012. **52**(5): p. 1199-1212.
91. Wang, J., T. Hou, and X. Xu, *Recent Advances in Free Energy Calculations with a Combination of Molecular Mechanics and Continuum Models.* Current Computer-Aided Drug Design, 2006. **2**(3): p. 287-306.
92. Liu, X., et al., *Mechanism of β2AR regulation by an intracellular positive allosteric modulator*. Science, 2019. **364**(6447): p. 1283-1287.
93. Lu, J., et al., *Structural basis for the cooperative allosteric activation of the free fatty acid receptor GPR40.* Nat Struct Mol Biol, 2017. **24**(7): p. 570-577.

94. Xiao, P., et al., *Ligand recognition and allosteric regulation of DRD1-Gs signaling complexes.* Cell, 2021. **184**(4): p. 943-956.e18.
95. Zheng, Y., et al., *Structure of CC chemokine receptor 2 with orthosteric and allosteric antagonists.* Nature, 2016. **540**(7633): p. 458-461.
96. Oswald, C., et al., *Intracellular allosteric antagonism of the CCR9 receptor.* Nature, 2016. **540**(7633): p. 462-465.
97. Liu, X., et al., *Mechanism of intracellular allosteric β2AR antagonist revealed by X-ray crystal structure.* Nature, 2017. **548**(7668): p. 480-484.
98. Liu, X., et al., *An allosteric modulator binds to a conformational hub in the β(2) adrenergic receptor.* Nat Chem Biol, 2020. **16**(7): p. 749-755.
99. Robertson, N., et al., *Structure of the complement C5a receptor bound to the extra-helical antagonist NDT9513727.* Nature, 2018. **553**(7686): p. 111-114.
100. Pandey, P., K.K. Roy, and R.J. Doerksen, *Negative allosteric modulators of cannabinoid receptor 2: protein modeling, binding site identification and molecular dynamics simulations in the presence of an orthosteric agonist.* J Biomol Struct Dyn, 2020. **38**(1): p. 32-47.
101. Chien, E.Y., et al., *Structure of the human dopamine D3 receptor in complex with a D2/D3 selective antagonist.* Science, 2010. **330**(6007): p. 1091-5.
102. Lane, J.R., et al., *Structure-based ligand discovery targeting orthosteric and allosteric pockets of dopamine receptors.* Mol Pharmacol, 2013. **84**(6): p. 794-807.
103. Feng, Z., et al., *Computational Advances for the Development of Allosteric Modulators and Bitopic Ligands in G Protein-Coupled Receptors.* The AAPS Journal, 2015. **17**(5): p. 1080-1095.
104. Liu, X., et al., *An allosteric modulator binds to a conformational hub in the β2 adrenergic receptor.* Nature Chemical Biology, 2020. **16**(7): p. 749-755.
105. Ramesh, K. and D.M. Rosenbaum, *Molecular basis for ligand modulation of the cannabinoid CB(1) receptor.* Br J Pharmacol, 2021.